Biogeosciences

Discussions

Nitrite Cycling in the Primary Nitrite Maxima of the Eastern Tropical North Pacific

Nicole M. Travis[1], Colette L. Kelly[1], Margaret R. Mulholland[2], Karen L. Casciotti[1]

[1] Earth System Science, Stanford University, Stanford CA, 94305, USA
[2] Department of Ocean, Earth and Atmospheric Science, Old Dominion University, Norfolk VA, 23529, USA

Correspondence to: Nicole M. Travis (ntravis@stanford.edu)

Abstract. The primary nitrite maximum (PNM) is a ubiquitous feature of the upper ocean, where nitrite accumulates in a sharp peak at the base of the euphotic zone. This feature is situated where many chemical and hydrographic properties have strong gradients and the activities of several microbial processes overlap. Near the PNM, four major microbial processes are active in nitrite cycling: ammonia oxidation, nitrite oxidation, nitrate reduction and nitrite uptake. The first two processes are mediated by the nitrifying archaeal/bacterial community, while the second two processes are conducted by phytoplankton. The overlapping spatial habitats and substrate requirements for these microbes have made understanding the formation and maintenance of the PNM difficult. In this work, we leverage high resolution nutrient and hydrographic data and direct rate measurements of the four microbial processes to assess the controls on the PNM in the Eastern Tropical Pacific. The depth of the nitrite maxima showed strong correlations with several water column features (e.g., top of the nitracline, top of the oxycline, depth of the chlorophyll maxima), whereas the concentration of the nitrite maxima correlated weakly with fewer water column features (e.g. nitrate concentration at the nitrite maximum). The balance between microbial rate processes active in nitrite cycling was a poor predictor of the concentration of the nitrite maximum, but rate measurements showed that nitrification was a major source of nitrite in the ETNP, while phytoplankton release occasionally accounted for large nitrite contributions near the coast. The temporal mismatch between rate measurements and nitrite standing stocks suggests that studies of the PNM across multiple time scales are necessary.

Short Summary (500 char.) The primary nitrite maximum is a ubiquitous upper ocean feature where nitrite accumulates, but we still do not understand its formation and the co-occurring microbial processes involved. Using correlative methods and rates measurements, we found strong spatial patterns between environmental conditions and depth of the nitrite maxima, but not the concentration of the maxima. Nitrification was a major producer of nitrite, with occasional high nitrite production from phytoplankton near the coast.

1 Introduction

Nitrogen (N) availability often controls ocean productivity through its role as a limiting nutrient. In marine systems, nitrate makes up over 88% of the bioavailable ('fixed') N pool, with dissolved organic N representing the next largest pool of fixed N (Gruber, 2008). However, the vertical distributions of these species render them unavailable to many

36   of the microbes that require them, e.g., nitrate is depleted in euphotic surface waters where primary production is
37   confined, but abundant in waters below the euphotic zone. Other inorganic fixed N species, e.g., nitrite and
38   ammonium, are present in smaller quantities, but their production and consumption are tightly coupled in the marine
39   environment. In the upper ocean, the nitracline demarcates a spatial transition where nitrate, nitrite and ammonium
40   may all be available to microbes simultaneously. In particular, the primary nitrite maximum (PNM) is a ubiquitous
41   feature of the upper ocean, where nitrite often accumulates to concentrations near 300 nM, although concentrations as
42   high as 2.8 μM have been reported (Brandhorst, 1958; Carlucci et al., 1970; Dore and Karl, 1996; GLODAP, V2;
43   Wada and Hattori, 1972). While in some cases nitrite can be present throughout the entire surface water column
44   (Lomas and Lipschultz, 2006; Zakem et al., 2018), nitrite concentrations are below detection in most of the ocean
45   because nitrite is an intermediate formed during oxidation of reduced N (NH_4^+, DON) (Zehr and Kudela, 2011; Zehr
46   and Ward, 2002). The accumulation of nitrite at the PNM occurs at a depth horizon where dynamic N cycling occurs
47   and can appear and disappear within the span of only 25 meters. The PNM location generally coincides not only with
48   the top of the nitracline, but also with the depth of the oxycline, the depth of the chlorophyll maximum, and just below
49   or coincident with an ammonium maximum near the base of the euphotic zone (Dore and Karl, 1996; Herbland and
50   Voituriez, 1979; Holligan et al., 1984; Kiefer et al., 1976; Zafiriou et al., 1992; Zakem et al., 2018). The consistent
51   strong spatial relationships between nitrite and both nitrate and chlorophyll concentrations hint at a relationship
52   between these environmental parameters and nitrite production, but does not provide a clear mechanism.

53   Because the PNM sits at a depth where many environmental parameters and microbial N transformations are in
54   transition, determining the exact controls on nitrite accumulation in the PNM remains difficult (Lomas and Lipschultz,
55   2006; Wan et al., 2021, 2018; Zakem et al., 2018). Near the PNM, the three main microbial groups involved in nitrite
56   cycling are bacterial and archaeal nitrifiers and phytoplankton. Nitrification comprises the oxidation of ammonia to
57   nitrate with nitrite as an intermediate. Archaeal ammonia oxidizers dominate the oxidation of ammonia to nitrite
58   (Francis et al., 2007, 2005; Mincer et al., 2007; Santoro et al., 2010; Schleper et al., 2005), while bacterial nitrite
59   oxidizers convert nitrite to nitrate (Lücker et al., 2013, 2010; Ward and Carlucci, 1985; Watson and Waterbury, 1971).
60   Many phytoplankton can also both produce and consume nitrite. Traditionally, phytoplankton are thought to be
61   consumers of inorganic N, but it is now well documented that they also release inorganic N, including nitrite (Al-
62   Qutob et al., 2002; Collos, 1998, 1982; Lomas and Glibert, 2000). Nitrification and photosynthesis co-occur near the
63   depth of the PNM, making it difficult to determine how microbes interact and transform nitrogen to produce the nitrite
64   concentrations observed, how microbial physiologies differentially respond to gradients in environmental conditions
65   and ultimately what factors influence the magnitude and depth of the PNM (Ward et al., 1989).

66   The combination of each microbial group's physiological responses to environmental parameters controls the vertical
67   profiles of concentrations of different N species and leads to accumulation of nitrite at the PNM. Imbalance between
68   the two steps of nitrification has been used to explain nitrite accumulation; variations in light levels may cause
69   differential photoinhibition or differential recovery from photoinhibition of nitrite oxidizers leading to accumulation
70   of nitrite (Guerrero and Jones, 1996; Olson, 1981). Ammonia oxidizing bacteria are less sensitive to light, have quicker
71   recovery times to light stress, and are active at higher rates under light stress compared to nitrite oxidizing bacteria

72   (Guerrero and Jones, 1996; Olson, 1981). Recent studies focusing specifically on the numerically dominant ammonia

73   oxidizing archaea (AOA), have shown high variation in light tolerance across AOA phylotypes which may explain

74   the lack of strong light inhibition of ammonia oxidation in some studies (Horak et al., 2018; Merbt et al., 2012; Smith

75   et al., 2014). Additionally, nitrification rates are substrate-dependent and constrained to places and times when

76   ammonia and nitrite are both available (Martens-Habbena et al., 2009). Nitrite is also taken up by phytoplankton but

77   this process is thought to be light dependent (Lomas and Glibert, 2000; Mulholland and Lomas, 2008). Nitrite release

78   from phytoplankton is also well documented in culture studies (Al-Qutob et al., 2002; Collos, 1998), but it is still

79   unclear whether nitrite release occurs during incomplete nitrate reduction under low light conditions when energy for

80   its complete assimilation is limited, under fluctuating high light conditions as a photoprotective mechanism, or as a

81   stress response (Collos, 1982; Kiefer et al., 1976; Lomas and Glibert, 1999, 2000; Wada and Hattori, 1971).

82   Accumulation of nitrite occurs when the rate of its production exceeds that of its consumption. Thus, the presence of

83   the PNM is an indicator of conditions where net production and consumption of nitrite are, or have recently been,

84   imbalanced (Wada and Hattori, 1971). The accumulation of nitrite in the PNM may provide valuable insight into the

85   balance of relative rates of microbial nitrite cycling in the upper ocean, as it indicates a zone where biologically

86   mediated processes are not in balance and may be experiencing differential inhibition or limitation. Rarely are the four

87   major microbial processes related to PNM formation (ammonia oxidation, nitrite oxidation, nitrate reduction and

88   nitrite uptake) measured simultaneously in the field. A few studies have measured both steps of nitrification

89   concurrently near the ETNP (Beman et al., 2013; Füssel et al., 2012; Peng et al., 2015; Santoro et al., 2013; Ward et

90   al., 1982). The few paired rate measurements that exist tend to show that ammonia oxidation rates exceed nitrite

91   oxidation rates in the PNM, suggesting nitrite oxidation is the rate limiting step in the reaction pair and a potential

92   mechanism for nitrite accumulation (Beman et al., 2013; Schaefer and Hollibaugh, 2017). However, the lack of paired

93   measurements focused on the sharp PNM boundaries limits our understanding of the coupling/uncoupling between

94   the two steps of nitrification or other processes affecting nitrite accumulation across these depths. Higher resolution

95   paired measurements will allow us to investigate how environmental gradients create vertical zonation in the relative

96   rates of nitrite-cycling processes that lead to nitrite accumulation within narrow depth horizons. Previous

97   investigations of the PNM have typically focused on nitrifier communities or phytoplankton communities separately,

98   although it is understood that the niches of these communities overlap, and that both may contribute to nitrite

99   accumulation. The studies that have measured both phytoplankton and nitrifier processes (Mackey et al., 2011;

100   Santoro et al., 2013; Wan et al., 2018; Ward, 2005) support the idea that physiological constraints and competitive

101   interactions between these groups drive resource use and nitrite accumulation (Smith et al., 2014; Wan et al., 2021;

102   Zakem et al., 2018).

103   Understanding the controls on rates of co-occurring nitrite cycling processes will help clarify the distributions of

104   microbial activity and how relative rates of these processes may change due to future environmental perturbations.

105   For example, understanding the controls on and patterns of nitrification in the surface ocean is critical for

106   understanding new production, as estimates suggest more than 30% of oceanic primary production is supported by

107   nitrate supplied by nitrification in the euphotic zone (Santoro et al., 2010; Ward et al., 1989; Yool et al., 2007). In

108 addition, the relative contributions of nitrification and phytoplankton activity to the formation of the PNM may also
109 be important for understanding the potential for nitrous oxide formation in the surface ocean (Burlacot et al., 2020;
110 Kelly et al., 2021; Plouviez et al., 2019; Santoro et al., 2011).

111 In the oligotrophic Eastern Tropical North Pacific (ETNP), the PNM occurs as a sharp peak located at the top of the
112 nitracline and within the waning slope of the primary chlorophyll maximum. The PNM also sits above a secondary
113 nitrite maximum (SNM) that occurs within the oxygen deficient waters below. To investigate the relative contributions
114 of nitrification and phytoplankton processes to net accumulation of nitrite at the PNM feature, we measured rates of
115 four microbially-mediated nitrite cycling processes (ammonia oxidation, nitrite oxidation, nitrate reduction and nitrite
116 uptake) in vertical profiles through the PNM. We analyzed spatial and regional variations in environmental conditions
117 and water column features associated with the PNM, as well as the rates of nitrite production and consumption.

118 **2 Methods**

119 **2.1 Hydrography and nutrient analyses**

120 This study is based on data collected from four cruises to the Eastern Tropical North Pacific between April 2016 and
121 June 2018 (RB1603 – *R/V Ronald Brown*, April 2016; SKQ201617s – *R/V Sikuliaq,* December 2016; SR1805 – *R/V*
122 *Sally Ride*, April 2018; and FK180624 – *R/V Falkor*, June 2018; Figure 1). The ETNP hosts one of the largest oceanic
123 oxygen deficient zones (ODZs) and is a region of active nitrogen cycling. Oxygen concentrations decline precipitously
124 from saturated surface water concentrations to nanomolar levels across the oxycline in much of the study area (Cline
125 and Richards, 1972), with oxygen deficient waters beginning as shallow as 15 m at some coastal stations. This study
126 focused on nitrite cycling in the upper water column near the PNM, and all rate data were collected in oxygenated
127 waters in or above the oxycline.

128 Fifty-three stations were occupied during these cruises, and hydrographic observations of temperature, salinity, and
129 oxygen were made using a CTD package (RB1603 – Sea-Bird SBE 11+ CTD, SKQ201617s/SR1805/FK180624 –
130 Sea-Bird SBE 911+ CTD). Fluorescence and photosynthetically active radiation (PAR) measurements were measured
131 at a subset of stations (RB1603 – LiCor Biospherical Photosynthetically Active Radiation Sensor/SeaPoint
132 Chlorophyll Fluorometer). Discrete water samples were collected from Niskin bottles mounted to the CTD rosette to
133 measure dissolved inorganic N concentrations. Nitrite and ammonium concentration measurements were typically
134 made immediately onboard the ship, while samples for nitrate concentration measurements were 0.22 μm filtered and
135 frozen in 60-ml HDPE bottles for analysis at a shore-based laboratory. During the 2016 cruise, a pump profiling
136 system (PPS; as described in Codispoti et al., 1991) was also deployed with a separate CTD package (Seabird SBE-
137 19+, WetStar Fluorometer) at all 16 stations.

138 For all cruises, nitrite concentrations were measured colorimetrically (Strickland and Parsons, 1972). Briefly, five ml
139 of sample water from each Niskin bottle was reacted with 200 μl each of sulfanilamide and N-(1-NAPHTHYL)-
140 ethylenediamine reagents, and absorbance at 543 nm was measured after a 10 min reaction time and converted to
141 concentration using a standard curve, with an overall precision of ±0.006 μM. Ammonium concentrations were

142 measured shipboard using a fluorometric method after derivatization with ortho-phthaldialdehyde (OPA) reagent
143 (Holmes et al., 1999). Samples and standards were reacted with OPA for ~8 hours at 4°C in the dark before
144 measurement. In 2016, samples for nitrate plus nitrite were collected from discrete depths using Niskin bottles
145 mounted to a CTD rosette and analyzed shipboard using an Astoria Pacific autoanalyzer according to the
146 manufacturer's specifications using standard colorimetric methods (Strickland and Parsons, 1972). In 2017, nitrate
147 plus nitrite samples were analyzed using standard colorimetric methods on a Technicon Autoanalyzer at the University
148 of Washington. In 2018, nitrate plus nitrite was measured after Cd reduction using a WestCo SmartChem 200 Discrete
149 Analyzer at Stanford University, with an overall precision of ±0.6 μM. Nitrate concentrations were calculated by
150 subtracting nitrite from the concentration of nitrate plus nitrite for all cruises. During the 2016 cruise (RB1603), cast
151 water from the pump profiling system (PPS) was pumped directly through a Fast Repetition Rate Fluorometer (FRRF)
152 for chlorophyll *a* fluorescence measurements and then to an Alpkem Astoria-Pacific rapid-flow analysis system for
153 near-continuous profiles of nitrate, nitrite, and ammonium concentrations at one measurement per second and binned
154 to every meter (Holmes et al., 1999; Sakamoto et al., 1990; Strickland and Parsons, 1972).

155 Water column profiles were analyzed to determine station-specific water column features (Table. 1). The depth of the
156 top of the nitracline (Z_{nit}) was identified as the inflection point between the nitrate-depleted surface waters and an
157 increase in nitrate concentration of 1 μM compared to a reference surface depth of 20 m (Cornec et al., 2021). In
158 addition, the standard nitracline depth (Z_{mnit}) was identified as where the nitrate gradient was steepest. Similarly, the
159 top of the oxycline (Z_{oxy}) was identified as the inflection point between oxygen-replete surface waters, using a
160 reference depth of 20 m, and a decrease in oxygen concentration of 5 μM. The standard oxycline depth (Z_{moxy}) was
161 where the oxygen gradient was steepest. Other station-specific water column features identified include depth and
162 concentration of the nitrite maximum (m and μM, respectively), depth and concentration of the chlorophyll maximum
163 (m and mg m^{-3}, respectively), depth and concentration of the ammonium maximum (m and nM, respectively) and the
164 depth of 1% surface photosynthetically active radiance (PAR) level (m). Concentrations/characteristics of these
165 variables specifically at the depth of the nitrite maximum were also calculated (e.g., nitrate concentration (NO3$_{pnm}$),
166 chlorophyll concentration (Chl$_{pnm}$), ammonium concentration (NH4$_{pnm}$), temperature (T$_{pnm}$), density (D$_{pnm}$), percent
167 of surface PAR (PAR$_{pnm}$), oxygen concentration (O$_{pnm}$). The Brunt-Väisälä frequency (BV$_{pnm}$) was calculated at the
168 PNM nitrite maximum (±8 m) using the equation $N = \sqrt{\frac{-g}{\rho} * \frac{d\rho}{dz}}$, where g is the acceleration due to gravity (m s^{-2}), z
169 is depth (m) and ρ is density (kg m^{-3}). Depth-integrated concentrations of nitrate, nitrite and ammonium (μmol N m^{-2})
170 were calculated for the euphotic zone (upper 120 m), capturing the entirety of the PNM feature.

Table 1. Water Column Feature Acronyms, Definitions and Units

Symbol	Definition	Unit
PNM	Primary nitrite maximum, whole feature	–
Chl$_{max}$	Concentration of the deep chlorophyll maximum	mg m^{-3}
NH4$_{max}$	Concentration of the ammonium maximum	nM

$NO2_{max}$	Concentration of the PNM nitrite maximum	μM
Z_{chl}	Depth of the deep chlorophyll maximum	m
Z_{nh4}	Depth of the ammonium maximum	m
Z_{no2}	Depth of the PNM nitrite maximum	m
Z_{nit}	Depth of top of the nitracline	m
Z_{mnit}	Depth of steepest gradient in nitracline	m
Z_{oxy}	Depth of the top of the oxycline	m
Z_{moxy}	Depth of steepest gradient in oxycline	m
Z_{pPAR}	Depth of 1% surface PAR	m
Chl_{pnm}	Chlorophyll concentration at the PNM peak	mg m^{-3}
$NH4_{pnm}$	Ammonium concentration at the PNM peak	nM
$NO3_{pnm}$	Nitrate concentration at the PNM peak	μM
T_{pnm}	Temperature at the PNM peak	C
D_{pnm}	Density at the PNM peak	kg m^{-3}
PAR_{pnm}	Percent of surface PAR at the PNM peak	%
O_{pnm}	Oxygen concentration at the PNM peak	μM
BV_{pnm}	Brunt Väisälä Frequency at the PNM peak	s^{-1}
NH4_Int	Depth integrated ammonium over upper 120m	nmol N m^{-2}
NO2_Int	Depth integrated nitrite over upper 120m	μmol N m^{-2}
NO3_Int	Depth integrated nitrate over upper 120m	μmol N m^{-2}
Chl_Int	Depth integrated chlorophyll over upper 120m	mg m^{-2}

171

2.2 Nitrite cycling rates

173 Rates of ammonia oxidation, nitrite oxidation, nitrate reduction and nitrite uptake were measured at 12 of the 53
174 stations occupied over 4 cruises from 2016-2018 (Fig. 1a); five stations from 2016, two stations in 2017, and five
175 stations in 2018. At each of these stations during a pre-dawn cast, 3-4 depths near the PNM were sampled based on
176 real-time CTD fluorescence data during the downcast, targeting depths both within the chlorophyll maximum and on
177 the upslope and downslope of its peak. When available, nitrite profiles from previous casts were consulted to guide
178 sampling based on the location of the PNM within the chlorophyll maximum.

179   Rate measurements for microbial nitrite cycling processes were made using ^{15}N-tracer incubation experiments. From

180   each depth, six clear 500-ml HDPE Nalgene bottles were triple-rinsed and filled directly from the Niskin bottle for

181   light incubations. Additionally, six 500-ml or 1-L amber HDPE Nalgene bottles were triple-rinsed and filled for paired

182   dark incubations. One of three ^{15}N-labeled nitrogen substrates ($K^{15}NO_3^-$ enriched at 99.5atm%, $Na^{15}NO_2^-$ enriched at

183   98.8atm% or $^{15}NH_4Cl$ enriched at 99.5atm%) was added to duplicate bottles to achieve enrichments of 200 nM ^{15}N.

184   After gentle mixing, a 60 ml subsample was Sterivex-filtered (0.22 μm pore size) using a syringe to determine initial

185   concentration and ^{15}N enrichment of the substrate pool. Approximately 10 ml was used for shipboard measurement of

186   the initial concentrations of total nitrite or ammonium (ambient concentration plus ^{15}N-labeled DIN addition). The

187   other 50 ml was frozen in a 60-ml HDPE bottle for measurement of total nitrate concentration and isotopic enrichment.

188   Each incubation bottle was placed in a deck-board incubator that approximated the ambient light level from the sample

189   collection depth using neutral density screening. The percent PAR in the incubators was recorded using a submersible

190   Licor PAR meter or an *in situ* HOBO light and temperature logger (~1%,~4%,~20% surface PAR). Incubators were

191   plumbed with flow-through surface seawater to maintain in situ water temperatures. However surface water

192   temperatures were often significantly warmer than those at collection depth and could have biased some of the

193   incubation results. Subsamples were collected from each incubation bottle after approximately 8, 16 and 24 hrs.

194   Samples were Sterivex-filtered (0.22 μm pore size) and filtrate frozen in 60-ml HDPE bottles for nutrient and isotope

195   analysis. At the end of the incubation (24 hr), the remaining ~300 ml of water was filtered onto a pre-combusted

196   (450°C for > 4 h) GF/F (0.7 μm) filter; the filter was folded and placed into a cryovial and stored at -80°C for later

197   analysis of particulate ^{15}N analysis at the University of Hawaii Isotope Lab. All seawater samples were stored frozen

198   until the time of isotopic analysis. Incubation bottles were acid washed and re-used for experiments using the same

199   ^{15}N substrate.

2.3 Isotope analysis and rate calculations

201   For estimates of ammonia oxidation, nitrite oxidation and nitrate reduction rates, samples collected from each

202   timepoint were analyzed for ^{15}N enrichment in the product pool for each process (Table 2). For each sample, the

203   product was converted to nitrous oxide either by bacterial (*P. aureofaciens*) conversion using the denitrifier method

204   (McIlvin and Casciotti, 2011; Sigman et al., 2001) or chemical conversion using the azide method (McIlvin and

205   Altabet, 2005). Isotopic analysis via the denitrifier method was used for measurement of $^{15}NO_X$ (ie. $^{15}NO_3^-$ + $^{15}NO_2^-$)

206   in ammonia oxidation and nitrite oxidation experiments. Measurements of nitrite oxidation required pre-treatment of

207   samples to remove any remaining ^{15}N-NO_2 prior to analysis of ^{15}N-NO_3 (Granger and Sigman, 2009). Briefly, 10 ml

208   of each sample was treated with 100 μl of 4% sulfamic acid in 10% hydrochloric acid for 15 min, after which the pH

209   was neutralized using 85 μl of 2M sodium hydroxide before proceeding with denitrifier method. Samples were

210   prepared in volumes targeting 20 nmoles nitrate plus nitrite. The azide method was used to prepare nitrite produced

211   from nitrate reduction experiments for isotopic analysis (McIlvin and Altabet, 2005). Nitrite was converted to nitrous

212   oxide by incubating for ~30 min with a 2M sodium azide solution in 20% acetic acid. The reaction was neutralized

213   with 6M sodium hydroxide prior to isotope analysis. Since nitrite product concentrations were low (<2 μM), a

214   significant portion of the nitrite in the samples was newly created from ^{15}N-labeled nitrate, thus carrier nitrite (5-10

215   nmoles) of known isotope value was added to dilute the ^{15}N enrichment and increase overall concentration of nitrite

216   in the samples before analysis. Samples were analyzed in volumes targeting 10 nmoles of nitrite.

217   The isotopic composition of the nitrous oxide produced from each sample was measured in the Casciotti Laboratory

218   at Stanford University using an isotope ratio mass spectrometer (Thermo-Finnigan Delta[PLUS] XP) fitted with a front-

219   end custom purge-and-trap gas purification and concentration system (McIlvin and Casciotti, 2011). Each set of 9

220   samples was bracketed with international reference materials to correct for instrument drift and sample size, and to

221   calibrate isotope values. USGS32, USGS34, and USGS35 (Böhlke et al., 2003) were used to calibrate nitrate isotope

222   analyses, and RSIL-N23, N7373 and N10219 (Casciotti et al., 2007) were used to calibrate nitrite isotope analyses.

223   For nitrate reduction samples, additional mass balance corrections were made to correct for the addition of nitrite

224   carrier to the product pool before calculation of rates. The denitrifier method for natural abundance nitrate isotope

225   analyses typically has a precision of better than 0.5‰ for $\delta^{15}N$ (McIlvin and Casciotti, 2011; Sigman et al., 2001),

226   although standard deviations are higher for isotopically enriched samples. Here, the mean analytical precision of $\delta^{15}N$-

227   NO_X, $\delta^{15}N$-NO_3, $\delta^{15}N$-NO_2 measurements of ^{15}N-labeled samples were ±4.2‰, ±4.6‰ and ±0.7‰, respectively,

228   corresponding to mean coefficient of variance (CV%) of 5.3%, 0.56% and 9.7%, respectively (Table 2).

229   **Table 2. Nitrite cycling reactant and product pools as analyzed by isotope rate mass spectrometry after conversion to**
230   **nitrous oxide via denitrifier or azide methods.**

Microbial Process	^{15}N-labeled Reactant	Prep Method	^{15}N-labeled Product	Mean Precision (‰)	Mean CV %
Ammonia Oxidation	NH_4Cl	Denitrifier	NO_3^-/NO_2^-	4.2	5.3
Nitrite Oxidation	$NaNO_2$	Sulfamic-treated + Denitrifier	NO_3^-	4.6	0.56
Nitrate Reduction	KNO_3	Azide w/carrier	NO_2^-	0.7	9.7

231   Rate calculations were made by tracking the increase in product ^{15}N over the incubation period (Ward, 1985). For

232   ammonia oxidation the equation is as follows:

233    $$V_{NH3} = \frac{\Delta[^{15}NOX]_{t8-t0}}{af^{15}NH3_{t0} \times \Delta t \times 24} \qquad\qquad (1)$$

234   where $\Delta[^{15}NOX]_{t8-t0}$ is the change in product [15]NO_X concentration between the start of the incubation and the 8 h

235   timepoint (nM), $af^{15}NH3_{t0}$ is the atom fraction of [15]NH_3 substrate available at the start of the incubation period, and

236   Δt is the change in time (hours). The ammonia oxidation rate, V_{NH3}, is reported in units of nM N day^{-1}. A similar

237   equation was used to calculate nitrite oxidation and nitrate reduction rates, substituting the appropriate substrate and

238   product species for each process (Table 1). The 16 h and 24 h time point samples were analyzed but not used to

239   calculate rates as experiments showed non-linear trends after 8 hours of incubation due to substrate depletion. Based

240   on a threshold increase in product $\delta^{15}N$ compared to the initial product, a theoretical detection limit was calculated to

241   estimate the rate which we can reasonably expect to discern from zero (Santoro et al., 2013). This calculation is

242   sensitive to both the $\delta^{15}N$ of the substrate pool, the concentration of the product pool, and the CV% for $\delta^{15}N$

243 measurements. The threshold for detectable change in product $\delta^{15}N$ was approximated using the maximum CV% for

244 each experiment. For example, if the standard deviation in replicates for a sample with a $\delta^{15}N$ of 25‰ was ±0.6, a

245 CV% of 2.4% was used as the theoretical detectable difference between initial and final ^{15}N enrichment in the product

246 pool. Where available, the maximum CV% for each experimental unit was used to calculate the theoretical limit of

247 detection for each depth (Table S1). The mean theoretical detection limits for ammonia oxidation, nitrite oxidation

248 and nitrate reduction were 0.5, 6.9, and 0.9 nM day^{-1}, respectively. Experimental bottle duplicates were conducted for

249 most rate measurements and those standard deviations are reported with the final rate data (Table S1).

250 Filters from nitrite uptake rate experiments were dried overnight and packed in tin capsules before shipment to the

251 Biogeochemical Stable Isotope Facility at the University of Hawaii, where samples were analyzed on a Thermo

252 Scientific Delta V Advantage isotope ratio mass spectrometer coupled to a Costech Instruments elemental analyzer.

253 Rate calculations relied on ^{15}N enrichment of the particulate organic nitrogen over the 24 h incubation period as in

254 Dugdale and Goering (1967). Uptake rates were calculated according to Dugdale and Wilkerson (1986) where the

255 initial ^{15}N atom percent fraction of the reactant pool was calculated assuming 0.3663 for the ^{15}N atom percent of the

256 ambient substrate pool and 98.8atm% $^{15}N\text{-}NO_2^-$ of the isotope tracer addition. Nitrite uptake rates may be

257 underestimated due to dilution of the substrate pool via regeneration over the 24 incubation period, and loss of tracer

258 to unmeasured DON pools (Bronk et al., 1994; Glibert et al., 2019). No correction was made for possible rate

259 enhancement due to tracer addition (Dugdale and Wilkerson, 1986).

2.4 Multiple Linear Regression Analysis

261 Multiple linear regression (MLR) models were built to assess the environmental variables that influence the depth and

262 magnitude of the PNM feature in the ETNP. The first set of MLR models ('full' models) used semi-continuous

263 measurements (temperature, density, oxygen, chlorophyll fluorescence, PAR, nitrate, nitrite and ammonium) from

264 CTD/PPS casts collected at 16 stations on the 2016 cruise to predict nitrite concentration. Nitrate, nitrite and

265 ammonium data were natural-log transformed to satisfy normal distribution assumptions of the multiple linear

266 regression analyses. Using the R package *leaps*, the model was optimized using a best-subsets selection of the full

267 variable set to maximize R^2 and minimize root mean squared error for each potential model size using 10-fold cross

268 validation to calculate test error for each sized model (optimization led to selection of 19 variables out of 27 possible

269 explanatory variables – 7 main and 20 single interactions terms) (Miller, 2020). The model size that minimized test

270 error was selected, and a best-subsets selection method was used to determine the optimal variable coefficients. MLR

271 coefficients from the optimized models were then used to predict nitrite concentration for station depth profiles in the

272 ETNP. Three variations on the 'full' model were made using data from: 1) all stations, 2) a subset of 'coastal' stations

273 (6, 7, 8, and 9) and 3) a subset of 'offshore' stations (13, 14, 15 and 16). Stations were identified as 'coastal' or

274 'offshore', based on concentration of the nitrite maxima, concentration of the chlorophyll maxima, and nitracline

275 depth. Not all stations proximal to the coastline were characterized as 'coastal' (Table S2a, b).

276 A second set of MLR models ('core' models) was built using a more limited set of core variables from the PPS data

277 that focused on phytoplankton and nitrifier physiology and metabolism (chlorophyll, nitrate, ammonium, oxygen and

278   percent PAR). These five environmental variables, their quadratic terms and single interaction terms were included

279   for 20 parameters in total. This model experiment was constructed to assess the relative importance of these core

280   variables between 'coastal' and 'offshore' stations; therefore, no model size optimization was used to limit variables.

281   Instead, optimized coefficients for all variables were determined, and variables that contributed less than 2% of total

282   R^2 in both regional models were discarded. In two cases, a variable that was discarded from one regional model was

283   added back to keep the variable list identical between both models for ease of comparison. In the coastal 'core' model,

284   the quadratic term for chlorophyll contributed less than 2% to total R^2 but contributed greater than 2% relative

285   importance within the offshore 'core' model, and was therefore retained in both models. In the offshore 'core' model,

286   PAR was initially removed during the optimization processes because it contributed less than 2% to model R^2, but

287   was ultimately retained because it contributed greater than 2% relative importance within the coastal 'core' model.

288   The relative percent importance of each variable was calculated by iterative random-ordered removal of each variable

289   to estimate percent contribution to total model R^2 using the *relaimpo* package in R (Grömping, 2006).

3 Results

### 3.1 PNM structure and environmental conditions

292   The typical PNM feature in the ETNP was a unimodal nitrite accumulation situated just below the chlorophyll

293   maximum and at the top of the nitracline (e.g., Fig. 1b, c). The PNM feature can be described using characteristics of

294   the PNM peak (i.e. nitrite maximum (μM) and depth of the nitrite maximum (m)) and an integrated nitrite quantity for

295   the whole PNM feature. Although nitrite can seasonally accumulate all the way to the surface in some regions (Zakem

296   et al., 2018), homogenous surface nitrite concentrations were not observed in this dataset. Across the ETNP study

297   region, stations showed similar relative water column structure in the upper 200 m, although the exact depth and

298   magnitude of features varied. Generally, the depth distribution of features from shallowest to deepest was the top of

299   nitracline, the chlorophyll maximum, the ammonium maximum then the Nitrite maximum (Fig. 1b, c). This set of

300   sequential features occurred near the base of the euphotic zone at most stations. Surface irradiance attenuated through

301   the water column and the depth of 0.1-1 % surface PAR ranged between 25 m and 150 m depth, with the deepest light

302   penetration at offshore stations. The chlorophyll maximum was usually found around the 1% surface PAR depth and

303   within the nitracline. However, there was variation in how deep the chlorophyll maximum sat within the nitracline, as

304   reflected in the amount of nitrate measured at the depth of the chlorophyll maximum (Table S2a). The depth of the

305   nitrite maxima tended to occur within the downslope of the chlorophyll maxima, while the rest of the water column

306   had very low concentrations of both N species. The depth horizon of the PNM was often narrow, with detectable

307   nitrite concentrations spanning only 30 m in some cases.

308   The depth of maximum nitrite in the PNM shoaled from an average depth of 103 m at offshore stations to 21 m near

309   the coast, closely following the shoaling nitracline. In density space, the depth of the nitrite maxima fell within a

310   narrower range, from 22.1 to 26.3 kg m^{-3}, with a mean density across the study region of 24.1 kg m^{-3}. The nitrite

311   maxima had an average concentration of ~600 nM, but a range spanning 60-1520 nM. Two types of stations ('coastal'

312   and 'offshore') were identified based on water column features. Coastal stations (e.g., 2016 PPS 6, 7, 8, 9) had higher

313 concentrations of nitrite at the nitrite maxima, shallower depths of the nitrite maxima, more nitrate and slightly more

314 chlorophyll and light at the depth of the nitrite maxima (Table. S2a). Coastal stations also had shallower oxyclines,

315 1% PAR depths, ammonium maxima and chlorophyll maxima compared to offshore stations. Depth-integrated

316 chlorophyll, nitrate and ammonium in the upper 120 m were higher at coastal stations. Offshore stations (e.g., 2016

317 PPS 13,14, 15,16) had deeper nitraclines, smaller chlorophyll maxima and less light at the depth of the nitrite maxima.

318 **Figure 1. Map of the ETNP region showing cruise tracks included in this study from four cruises from 2016-2018 (a).**
319 **Stations where rate measurements were made are marked with white stars. Pump profile data was collected at each station**
320 **occupied during the 2016 cruise. Mean water column profiles from example 'coastal' stations (8 and 9) and example**
321 **'offshore' stations (14 and 16) during the 2016 cruise (b, c). Dashed grey line depicts the depth at which dissolved oxygen**
322 **concentrations declined below 3 μM.**
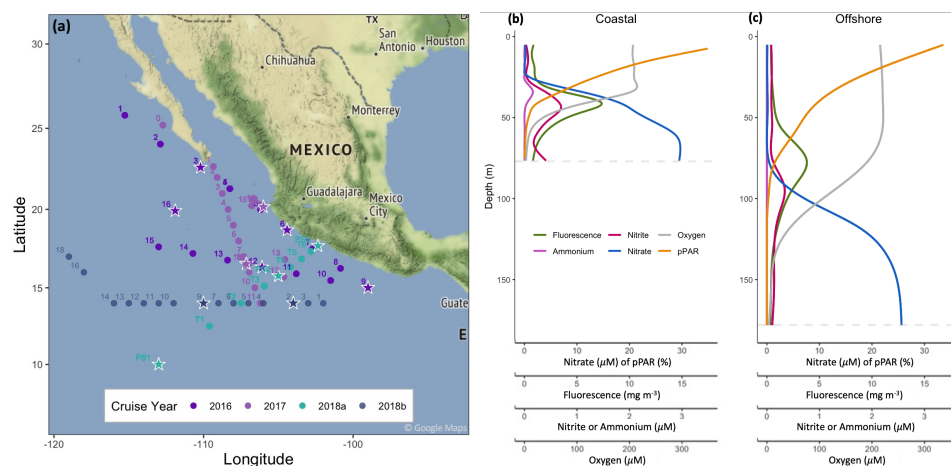
324 **3.2 Regressions with the nitrite maxima**

325 There were no strong linear correlations between the concentrations of nitrite and other observed environmental

326 variables in vertical profiles (chlorophyll, depth, density, oxygen, temperature, nitrate, ammonium) (Fig. S1). This is

327 unsurprising since the features with unimodal profiles (chlorophyll, ammonium) have concentration maxima that are

328 offset vertically from the nitrite maxima, and features with other distributions (eg. exponential) are not expected to

329 have linear relationships with a unimodal nitrite profile. However, spatial relationships between environmental

330 gradients are still observed in the quantity regressions; for example, the density regression clearly shows that the peak

331 of the PNM feature consistently fell near 24 kg m^{-3} isopycnal across the region in 2016 (Fig. S1).

332 To better match unimodal nitrite profiles with spatially offset and vertically non-unimodal environmental gradients,

333 station-specific features were identified in the high-resolution 2016 PPS profiles and, where possible, in the CTD

334 datasets (Table 1, e.g., concentration of the nitrite maxima and depth of nitrite maxima). The concentrations of the

335 nitrite maxima (μM) were regressed against the magnitude of other station features (Fig. 2). The strongest correlation

336 ($R^2 = 0.50$, p<0.01) appeared between the concentration of the nitrite maxima and the nitrate concentrations at the

337 nitrite maxima (Fig. 2c). The Brunt-Väisälä frequency (BV), related to water column stability, also had a strong

338 positive correlation ($R^2 = 0.40$, p<0.01) with the concentration of the nitrite maxima (Fig. 2l). There were weaker

339 correlations with other parameters such as the concentration of the chlorophyll maxima (mg m^{-3}), temperature (°C) at

340 the depth of the nitrite maxima and oxygen concentration (μM) at the depth of the nitrite maxima (R^2 = 0.23, 0.25,

341 0.29, respectively, all p< 0.04) (Fig. 2a, h, f). The nitrite maxima were not linearly correlated with percent surface

342 PAR (%) at the depth of the nitrite maxima or the concentration of ammonium (nM) at the depth of the nitrite maxima

343 (Fig. 2g, d). Depth-integrated chlorophyll, nitrate, and nitrite concentrations in the upper 120 m (excluding ODZ

344 waters with O$_2$ < 3 μM) were higher when the nitrite maximum was larger (Fig. 2i, j, k). The nitrite maxima did not

345 correlate with depth-integrated ammonium concentrations (not shown). Inclusion of lower resolution CTD casts from

346 cruises in 2017/2018 decreased the strength of the linear correlations, likely because of larger error in determining

347 water column features (e.g., depth of the nitrite maxima, top of nitracline) with larger (~10 m) spacing between discrete

348 measurements (Fig. S2a).

349 **Figure 2. Linear regression of concentration of the nitrite maxima against concentrations of water column features,**
350 **integrated amounts of chlorophyll and DIN, and Brunt-Väisälä frequencies using PPS station data from 2016 (n=16).**
351 **Chlorophyll concentration at the depth of the nitrite maxima (a), concentration of the chlorophyll maxima (b), nitrate**
352 **concentration at the depth of the nitrite maxima (c), ammonium concentration at the depth of the nitrite maxima (d),**
353 **concentration of the ammonium maxima (e), oxygen concentration at the depth of the nitrite maxima (f), percent surface**
354 **irradiance at the depth of the nitrite maxima (g), temperature at the depth of the nitrite maxima (h), integrated chlorophyll**
355 **through the top 120m (i), integrated nitrate through the top 120m (j), integrated nitrite through the top 120m (k), and the**
356 **Brunt-Väisälä frequency across the density gradient ±8m around the depth of the nitrite maxima (l).**
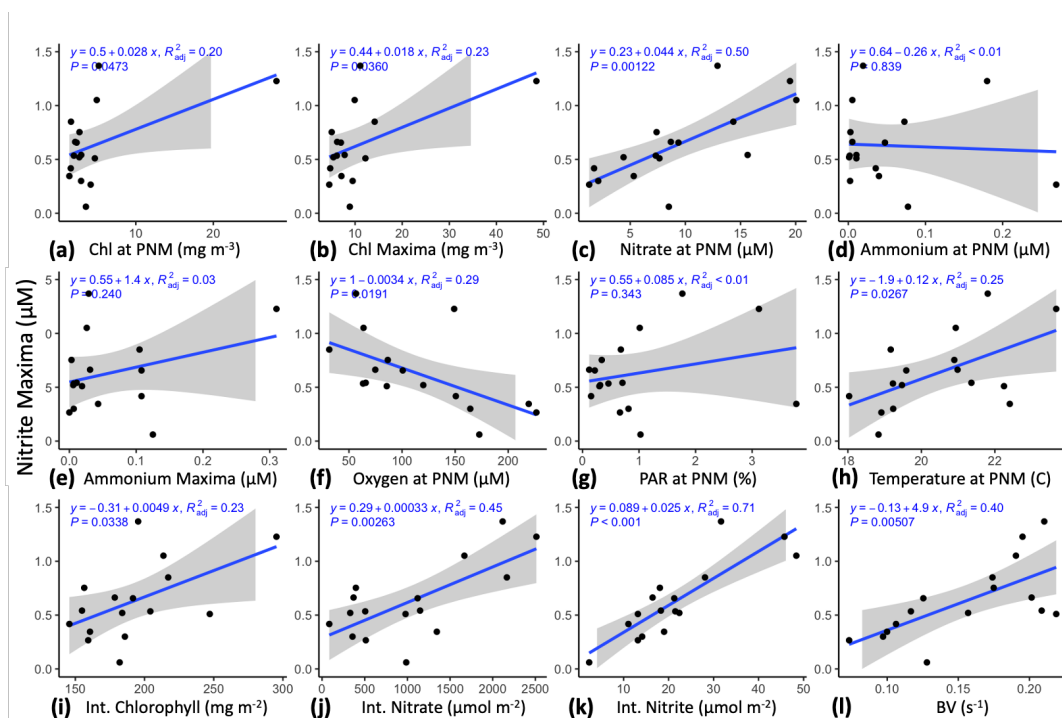

357

358 **3.3 Regressions with depth of the nitrite maxima**

359   The depth of the nitrite maximum at each station was also regressed against the depth of station-specific features (Fig.

360   3). All water column features showed strong linear correlations with the depth of the nitrite maxima (Fig. 3 a-h). The

361   top of the nitracline and the depth of 1% PAR had the strongest correlations with the depths of the nitrite maxima (R^2

362   = 0.94, 0.85) (Fig. 3b, g). Correlation of depths of the nitrite maxima with midpoint-calculated oxyclines and

363   nitraclines was weaker, possibly because those features are less easily defined, or the steepness of these "clines" were

364   still actively being shaped by the biological responses to changing physical and environmental forcing. The depths of

365   the nitrite maxima tended to be related to the depth locations of other features and were not as strongly correlated with

366   the magnitudes of any other feature (Fig. S3). However, the depth of the nitrite maxima and the concentration of the

367   nitrite maxima were mildly correlated ($R^2 = 0.22$, p = 0.039), with larger nitrite maxima tending to occur at shallower

368   depths. This correlation became insignificant when the CTD data were included (Fig. S2b). Integrated nitrate had a

369   strong correlation with the depth of the nitrite maxima ($R^2 = 0.88$, p < 0.01), which is reflective of the depth of the

370   nitrite maximum tracking with the top of the nitracline. Depth-integrated chlorophyll and nitrite concentrations had

371   more moderate correlations with the depths of the nitrite maxima ($R^2 = 0.21$, p = 0.041 and $R^2= 0.32$, p = 0.013,

372   respectively). Depth-integrated ammonium concentrations did not correlate with the depth of the nitrite maxima.

373   **Figure 3. Linear regression of depths of the nitrite maxima against water column features from data collected during the**
374   **2016 cruise using the PPS. Depth of the nitrite maxima was regressed against: a) nitracline depth (m), b) top of the nitracline**
375   **(m), c) oxycline depth (m), d) top of the oxycline (m), e) depth of the chlorophyll maxima (m), f) depth of the ammonium**
376   **maxima, g) depth of 1% surface irradiance, h) concentration of the nitrite maxima (μM), i) integrated chlorophyll through**
377   **the top 120m j), integrated nitrate through the top 120m k), integrated nitrite through the top 120m and l) integrated**
378   **ammonium through the top 120m. PPS station data from 2016 (n=16).**


379
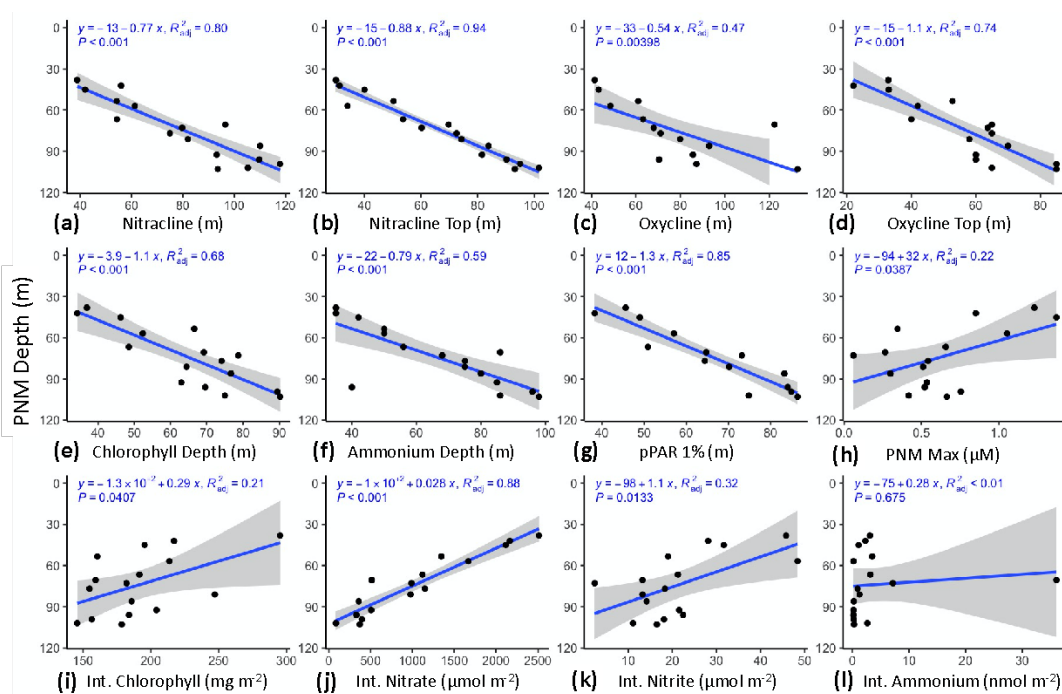
3.4 Nitrite Cycling Rates

Rates of nitrite cycling determined for the four major nitrite cycling processes near the PNM were within the same range as previous measurements made in the ETNP region and along the adjacent California coast (Beman et al., 2008; Santoro et al., 2013, 2010; Ward et al., 1982). Within our dataset, the mean rates of ammonia oxidation and nitrite oxidation were similar to each other (23.7±3.5 and 19.4±3.0 nM day^{-1}, respectively), although there was a large range in individual rate measurements across stations and depths, with maximum rates reaching 85.3 and 81.0 nM day^{-1} respectively. Rates of the two phytoplankton-based processes were generally lower and not as similar to each other, with a mean nitrite uptake rate of 19.0±5.3 nM day^{-1} and mean nitrate reduction rate of 6.1±1.9 nM day^{-1}. However, nitrite uptake reached one of the highest rates measured at 165 nM day^{-1}, and the nitrate reduction rate reached 53.2 nM day^{-1} at a coastal station during the 2017 winter cruise. The pooled mean standard deviation across experimental bottle replicates for ammonia oxidation, nitrite oxidation and nitrate reduction were 3, 4.6 and 1 nM day^{-1}, respectively (Table S1).

Figure 4. Aggregated rate measurements from 2016-2018 with respect to density (sigma T); ammonia oxidation, nitrite oxidation, nitrite uptake and nitrate reduction (panels a-d, respectively) (nM day^{-1}), ammonium (nM), nitrite and nitrate (μM), and net nitrite production (nM day^{-1}) (panels e-h, respectively), and net consumption, net production, net nitrite production from phytoplankton and net nitrite production from nitrification (nM day^{-1}) (panels i-l, respectively). Measurements are colored by relative depth to the station-specific nitrite maximum; above the depth of the nitrite maximum (green crosses), at the nitrite maximum (magenta circles) or below the station-specific depth of the nitrite

398   **maximum (blue triangles). The mean ETNP nitrite maxima isopycnal (24.1 kg m⁻³) is marked as a horizontal dashed line**
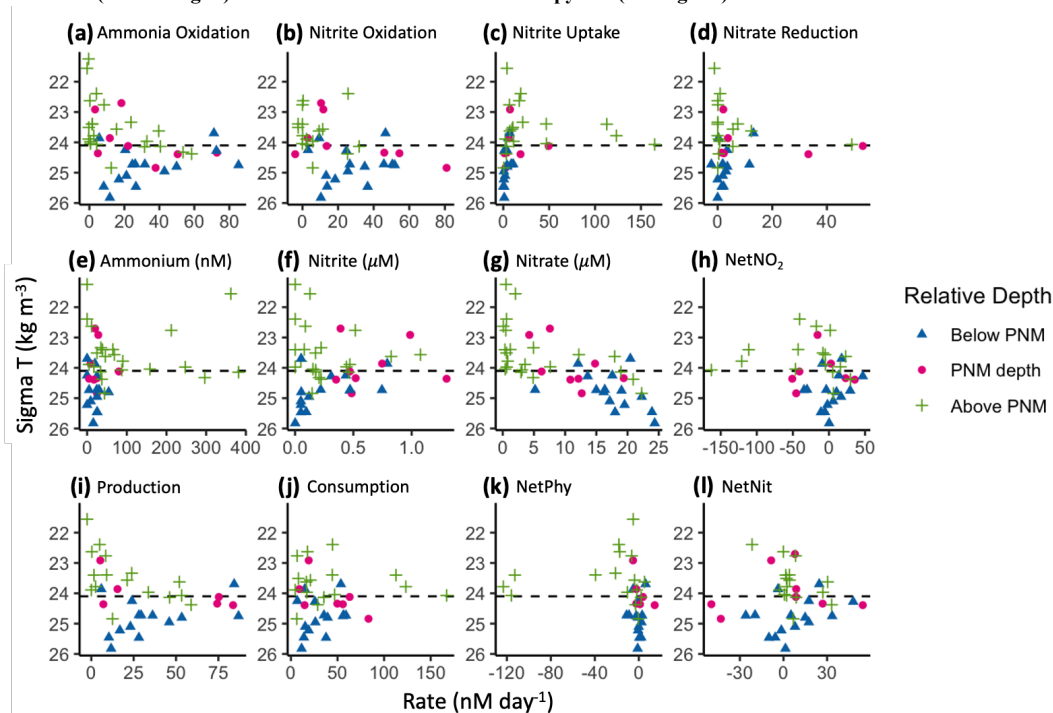
399

400   When plotted in density space to aggregate data across years and stations, all processes showed rate maximum at a

401   subsurface density layer (Fig. 4). Nitrifier processes (ammonia oxidation (Fig. 4a) and nitrite oxidation (Fig. 4b)), had

402   maximal rates near, or just below, the average density layer for the nitrite maxima across this region (24.1 kg m⁻³).

403   Nitrite uptake (Fig. 4c) and nitrate reduction (Fig. 4d) rates reached their maxima just above the mean nitrite maxima

404   isopycnal. Nitrification rates were highest in the lower half of the nitracline, while phytoplankton-mediated processes

405   (nitrite uptake and nitrate reduction) were highest on the upper slope of the nitracline where nitrite and ammonium

406   concentrations tended to be higher and light available. While the highest activities of the two microbial groups were

407   spatially segregated, within-group production and consumption processes had maxima at similar depths. All four rates

408   formed vertically unimodal distributions, but there was still a large range in measured rates near the peaks with many

409   rates close to zero.

410   Net nitrite production from nitrification alone (NetNit = ammonia oxidation – nitrite oxidation) ranged from -49.6 to

411   54.5 nM day⁻¹ with a mean of 5.5±3.1 nM day⁻¹ (Fig. 4I). The majority of NetNit values were positive, and maximal

412   rates were observed just below the mean nitrite maxima isopycnal. Negative NetNit values were driven by high nitrite

413   oxidation values. Net nitrite production from phytoplankton processes (NetPhy = nitrate reduction - nitrite uptake)

414   were typically low (mean -13.3±4.9 nM day⁻¹), with many negative values resulting from rates of nitrite uptake that

415   were generally higher than nitrate reduction (Fig. 4k). The largest negative values occurred above the mean nitrite

416   maxima isopycnal, driven by high nitrite uptake rates where light concentrations were high and nitrate low in the

Biogeosciences
Discussions

417   surface waters. Below the mean nitrite maxima isopycnal, NetPhy remained near zero because both nitrite uptake and

418   nitrate reduction rates were low. The largest positive NetPhy value was at a coastal station (14 nM day^{-1}), where nitrate

419   reduction reached 33.2 nM day^{-1}, but NetPhy was typically an order of magnitude smaller than NetNit.

420   The vertical distributions of total nitrite production (production = ammonia oxidation + nitrate reduction, Fig. 4j) and

421   total nitrite consumption (consumption = nitrite oxidation and nitrite uptake, Fig. 4k) showed maximal rates near the

422   mean nitrite maxima isopycnal (24.1 kg m^{-3}). Total nitrite production peaked just below the mean nitrite maxima

423   isopycnal, with a maximum value of 87 nM day^{-1}. Total nitrite consumption peaked just above the mean nitrite maxima

424   isopycnal, with a maximum value of 167 nM day^{-1}. The higher consumption rates just above the mean nitrite maxima

425   isopycnal were due to higher nitrite uptake rates, especially at coastal stations (Fig. 4c). There was a large range in

426   rates of nitrite production and consumption processes, but mean values were of similar magnitude (26.4 nM day^{-1} and

427   39 nM day^{-1}, respectively). Total net nitrite production (NetNO$_2$, difference between total production and total

428   consumption) was highest near the PNM. Negative net nitrite production rates occurred throughout the whole water

429   column, reflecting high nitrite uptake above the mean nitrite maxima isopycnal and high nitrite oxidation values below

430   the mean nitrite maxima isopycnal (Fig. 4h). The mean of positive NetNO$_2$ values was 16.7 nM day^{-1} (rates > -2 only,

431   n=17), although mean NetNO$_2$ was -14.2 nM day^{-1} when all data points were included. The maximum rate of NetNO$_2$

432   was slightly lower than NetNit alone (46.9 vs 54.5 nM day^{-1}, respectively), but the peaks of the vertically unimodal

433   distributions occurred at the same depths.

434   While the aggregated rates of NetNO2 peaked near the mean nitrite maxima isopycnal for the region, neither NetNO2

435   (nor any individual rates) were able to predict the observed nitrite concentrations. Simple linear regressions of each

436   rate, or calculated net rates, against the quantity of nitrite did not show significance (Fig. S4). Limiting the regression

437   to a single nitrite maximum and a single highest rate per station also did not show any linear correlation (Fig. S5).

438   However, some qualitative patterns were noticeable, where the highest rates of phytoplankton-based processes

439   occurred in samples with lower nitrite concentrations (shallower in the water column). The highest nitrite uptake rates

440   (>25 nM day^{-1}) appeared to restrict the maximum nitrite quantity below 500 nM. Conversely, when high nitrite

441   concentrations were measured (>600 nM), nitrite uptake rates were low, never higher than 10 nM day^{-1}. Nitrate

442   reduction rates were also higher at lower nitrite concentrations. The highest ammonia oxidation rates (>40 nM day^{-1})

443   were found where nitrite concentrations were <500 nM (Fig. S4). Nitrite concentrations were highest (>600 nM) where

444   ammonia oxidation rates were lower (<40 nM day^{-1}). The highest nitrite concentrations were associated with waters

445   having lower nitrite oxidation rates (<20 nM day^{-1}), although there were more outliers in this regression. Thus,

446   although nitrification was an important contributor to total nitrite production, the instantaneous rates could not be used

447   to predict nitrite concentrations nor could maximum rate at a station predict the nitrite concentration at the nitrite

448   maxima.

449   Assuming approximate steady state for PNM nitrite concentrations, rate measurements can be used to calculate a

450   potential residence time for nitrite across the PNM feature. Using total nitrite production and nitrite concentrations,

451   the mean residence time was 30.4 days. However, there was a wide range in residence times across all samples,

452   particularly those from above the average nitrite maxima isopycnal for the region (Fig. S6a). Using total consumption

453   rates in the calculation gave a slightly lower mean residence time for the region (20.3 days), but again had a large

454   range in residence times above the mean nitrite maxima isopycnal (0.01-103.2 days) (Fig. S6c). The discrepancy in

455   residence times calculated using the influx and outflux terms for the nitrite pool suggests that the PNM feature was

456   most likely not in steady state (as also suggested by the high variation in measured rates at the PNM and inability of

457   rates to correlate with observed nitrite accumulation), with differences in the dynamics above and below the nitrite

458   maxima.

459   **3.5 Contribution from Nitrification**

460   In considering the metabolisms responsible for accumulation of nitrite at the PNM, it is important to consider the

461   distribution and magnitude of nitrite production processes vertically through the water column as well as their relative

462   contributions to total nitrite production. At our sites in the ETNP, ammonia oxidation contributed over 70% of the

463   total nitrite production through most of the water column (Fig. 5a). The stations where ammonia oxidation contributed

464   less to total nitrite production were typically coastal stations with low ammonia oxidation rates (e.g., <2 nM day^{-1}) or

465   with high nitrate reduction rates (>20 nM day^{-1}). These results support the idea that both ammonia oxidation and

466   nitrate reduction can contribute to nitrite production, but that the dominant source was from ammonia oxidation at

467   most stations, particularly at the depth of the nitrite maxima and below. For nitrite consumption, nitrite oxidation

468   contributed greater than 70% of total nitrite consumption below the mean density layer of the nitrite maxima. Above

469   the mean density layer of the nitrite maxima, the contribution to total nitrite consumption from nitrite oxidation became

470   more variable, but with most values below 70% due to more nitrite uptake. Particularly low contributions to total

471   nitrite consumption from nitrite oxidation were seen above the depth of the nitrite maxima at coastal stations where

472   nitrite uptake rates were highest. Potential decoupling of ammonia and nitrite oxidation could be seen in the upper

473   water column, with NetNit peaking at the depth of the nitrite maxima (Fig. 4l), which is more difficult to discern in

474   the individual ammonia oxidation and nitrite oxidation rates (Fig. 4a,b).

475   **Figure 5. Percent contribution of nitrification to total nitrite production (a) and total nitrite consumption (b) across density**

476   **space. Measurements are colored by relative depth to the station-specific nitrite maximum; above the depth of the nitrite**

477 **maximum (green crosses), at the nitrite maximum (magenta circles) or below the station-specific depth of the nitrite**
478 **maximum (blue triangles). The mean ETNP nitrite maxima isopycnal (24.1 kg m⁻³) is marked as a horizontal dashed line**


479
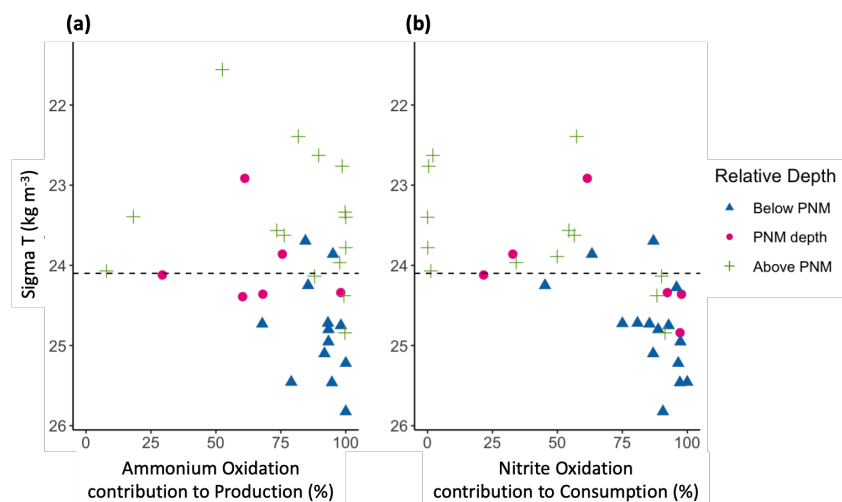
3.6.1 'Full' model PNM predictions using all stations

The 'full' model multiple linear regression optimization across all stations resulted in a combination of 10 variables that were able to predict 66% of the total variance in nitrite concentration (Fig S7a). The final optimized model included 3 primary variables (chlorophyll, ammonium and oxygen) and 7 interaction terms (Table S3). Based on relative importance calculations, the temperature-density interaction term contributed the largest amount to the total variance in nitrite explained by the model (19.8%). The top 3 variables by relative importance all involved temperature, and in sum contributed 32.3% to the total model R^2. Eight out of ten of the variables selected in this model contributed less than 6% each to total model R^2 (Table S3). The predicted vs. observed nitrite slope was less than 1, meaning small nitrite maxima ($<\sim70$ nM) were overpredicted and larger nitrite maxima tended to be underpredicted (Fig. S7a).

The all-station 'full' model predicted the depth of the nitrite maxima well (mean depth error = 3.7 m) and underpredicted the nitrite maxima by an average of 230 nM across all stations (when the extreme over-prediction of 15 µM at Station 8 was omitted) (Fig. 6, Table S4). The accuracy of the all-station model varied across station types, with the most accurate stations including an assortment of coastal, offshore and other (3,4 10,11,13).

Figure 6. Predicted nitrite profiles from the 'full' MLR models. Observed nitrite (deep pink), all-station model (purple), coastal model (green), offshore model (blue). Coastal stations used for training the coastal model (6, 7, 8, 9) are boxed in green and offshore stations used for training the offshore model (13, 14, 15, 16) are boxed in blue. Note: Scale is adjusted to compare PNM shapes between observations and models, and model maxima may be greater than 1.5 µM. See Table S5

498 **for model error values and Fig S9 for rescaled profiles.**

499
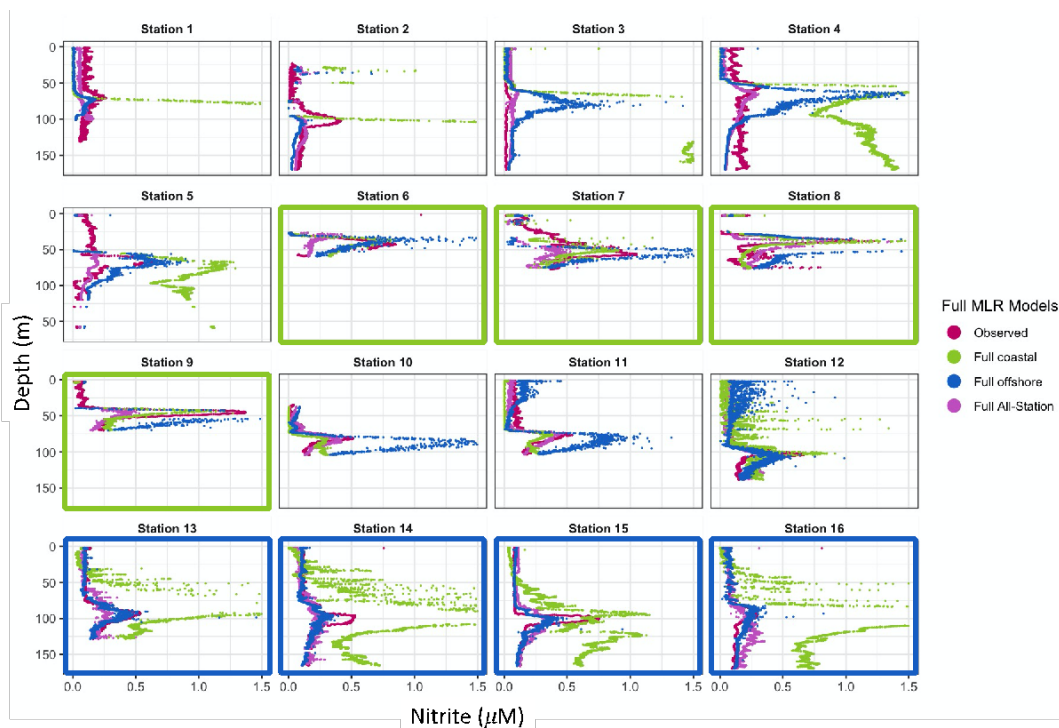
3.6.2 'Full' model PNM predictions using coastal stations

501 For the coastal 'full' model the optimization resulted in 10 variables and was able to predict 77% of the total

502 variance in nitrite across the coastal stations. The predicted versus observed slope was less than 1, suggesting

503 slight overprediction of smaller nitrite maxima (<330 nM) and slight underprediction of larger nitrite maxima

504 (Fig. S7). The most important variable was the nitrate-oxygen interaction term, which explained 17% of the total

505 model variance. Although nitrate was not included as a primary variable, it was involved in three out of seven

506 of the interaction terms, and in sum these nitrate interaction terms contributed to nearly half of the total model

507 R^2 (33.8%).

508 The coastal 'full' model was able to predict the depth of the nitrite maxima well at the coastal stations, with an

509 average underprediction in depth of only 2.9 m (Fig. 6, Table S4). The concentration at the nitrite maxima at

510 coastal stations was also accurately predicted by the coastal model, with an average underprediction of only 121

511 nM. The largest observed nitrite maxima (Station 8) were slightly overpredicted by this model, while the nitrite

512 maxima at Stations 6 and 7 were well predicted (Fig. 6, green). When applied to non-coastal stations, the coastal

513 'full' model overpredicted (>2x) the nitrite maxima (except Stations 10,11,12), with an average overprediction

514 for the whole region of ~1.13 µM (Table S4). The inability of this model to be applied across all stations is

515   reflected again in the poor correlation between observed and predicted nitrite (R^2=0.013, Fig. S7d). The coastal

516   'full' model predicted a double peak structure at 5 non-coastal stations (4, 5, 10, 13, 15). This PNM shape has

517   been observed in the field previously (Lomas and Lipschultz, 2006), and was also observed at stations 5 and 10

518   in our field data. Stations 4, 13 and 15 did not show a double peaked profile, even though it was predicted by the

519   coastal model.

3.6.3 'Full' model PNM predictions using offshore stations

521   For the offshore 'full' model, 12 variables were included after the optimization process and the final model

522   explained 79% of the overall variance in nitrite across offshore stations. The predicted vs observed slope was

523   less than 1, again suggesting slight overprediction of smaller nitrite maxima (<~150 nM) and slight

524   underprediction of larger sized nitrite maxima (Fig. S7c). The two most important variables in the offshore model

525   were the oxygen-chlorophyll and density-chlorophyll interaction terms, which each explained 9.4% of the total

526   nitrite variance (Table S3c). Chlorophyll appeared to be an important parameter in this model, being included as

527   a primary variable and in 4 interaction terms for a total contribution of 38% to total model R^2.

528   The offshore 'full' model predicted the depth of the nitrite maxima well for offshore stations, with a mean

529   underprediction in depth of only 0.3 m (Fig. 6, Table S4). The offshore model underpredicted the concentration

530   of the nitrite maxima by only 53 nM on average. Predicted nitrite profiles accurately captured the concentration

531   of the nitrite maxima at offshore stations 13 and 16, while offshore stations 14 and 15 were both slightly

532   underpredicted. The accuracy of the offshore 'full' model applied to all stations was much more variable, with

533   a mix of fairly accurate (5,12), overprediction (3,4,6,7,8,10,11) and underprediction (1,2) (Fig. 6, Fig. S7). Mean

534   overprediction of the offshore 'full' model applied across all stations was 855 µM, driven by an extreme

535   overprediction at Station 8 which when excluded makes the mean size error only 1.23 µM. The offshore model

536   predicts a slight double peak shape at Stations 5 and 8 only.

3.7 Multiple Linear Regression – 'core' model PNM predictions

538   A subset of 'core' variables was selected and applied in a second MLR analysis in order to directly compare the

539   influence of each variable between two regions (Coastal vs Offshore stations) (See Methods). There were 7 variables

540   included in the final 'core' models, with 4 primary variables, 1 quadratic term and 2 interaction terms (Table 2). In

541   both regional models, nitrate was involved in explaining the most variance (40.8% in the coastal model, 38.8% in the

542   offshore model).

543   **Table 2. Coefficients and relative importance from core models; coastal (a) and offshore (b)**

(a)

Coastal 'Core' MLR Coefficients

Variable	Coefficient	Percent Importance
Oxygen-Nitrate	0.0028	18.9
Nitrate	-0.4137	12.2
pPAR	-0.0183	12.1
Chl-Nitrate	0.0538	9.7
Chlorophyll	-0.0837	4.6
Oxygen	-0.0047	4.6
Chlorophyll2	-0.0014	2.3

(b)

Offshore 'Core' MLR Coefficients

Variable	Coefficient	Percent Importance
Chl-Nitrate	0.0752	16.7
Oxygen-Nitrate	0.0029	11.9
Chlorophyll	0.46	11.1
Oxygen	-0.0124	11
Nitrate	-0.7093	10.2
Chlorophyll2	-0.0994	6.8
pPAR	-0.0012	4.4

544

3.7.1 Coastal 'core' model

The coastal 'core' model was able to explain 83% of the variance in coastal nitrite concentration. The top 3 variables (oxygen-nitrate, nitrate, and pPAR) explained over half of the total model variance (44.1%). Nitrate was the dominant variable, with the combined contribution of all 3 nitrate variables explaining 41.9% of model variance. The total contribution of the chlorophyll related variables was 17.5%. The slope of the predicted vs observed values was 0.71, less than 1, indicating a tendency to overpredict the size of smaller nitrite maxima (< ~350 nM) and underpredict larger sized nitrite maxima (Fig. S8a).

In general, the coastal 'core' model predicted depth well, but was less accurate for nitrite maxima and general shape (Fig. 7). The coastal 'core' model underpredicted the depth of the nitrite maxima at coastal stations (-1.7 m), and underpredicted coastal nitrite maxima by an average of 208 nM, with a large range in error (-830 to +811 nM) (Table S5). Applying the coastal model to the full set of 16 stations showed that the coastal 'core' model overpredicted and underpredicted the nitrite maxima at non-coastal stations, as well as predicting a wide PNM shape that extends deeper in the water column than observed (Fig. 7). The predicted depths of the nitrite maxima from this coastal model fit well with the depth of the observed nitrite maxima, with a mean depth overprediction of only 2.3 m, with a single large outlier at Station 1 where depth was overpredicted by 23.4 m (Fig. 7, Table S5). On average, the coastal model overpredicted the nitrite maxima by just 12 nM across the region. However, there is a wide range in direction of prediction error, with Station 8 being overpredicted by 810 nM and Station 9 underpredicted by 830 nM.

3.7.2 Offshore 'core' model

The offshore 'core variable' model was able to explain 98% of the total variance in nitrite (natural-log transformed) at all offshore stations. The relative importance calculation of each variable shows that nitrate, chlorophyll and oxygen together explain more than a third of the total model variance (32.3%). These 3 single variables were also relatively similar in their individual contributions to total model variance (10.2%, 11.1%, 11%) (Table 2). However, nitrate was involved in both interaction terms, which were the top 2 most important variables. The combined contribution of all nitrate effects was 38.8%, almost half of the total model R^2 and similar to the coastal 'core' model. The total contribution of chlorophyll related variables is 34.6%, higher than that seen in the coastal 'core' model. The slope of predicted vs observed nitrite was less than 1, indicating a tendency to overpredict the size of smaller nitrite maxima and underpredict larger sized nitrite maxima with a cross-over point between over- and underprediction occurring at ~150 nM nitrite (Fig. S8).

573 In general, the offshore 'core' model predicted the depth of the nitrite maxima well, but less accurately predicted the

574 concentration of the nitrite maxima (Fig. 7). The depth of the nitrite maxima at offshore stations was overpredicted by

575 an average of 2.8 m, and the nitrite maxima was underpredicted by 82 nM at offshore stations. Applying the offshore

576 model across all 16 stations showed that the offshore core model tended to underpredict the nitrite maxima across the

577 region. The predicted depth of the nitrite maxima was an average of 5.5 m deeper than the observed depth of the nitrite

578 maxima, with a range in over and underpredictions from 18.6 m to 5.5 m respectively. The predicted concentration of

579 the nitrite maxima was lower than observations by an average of 218 nm across the region (Table. S4).

580 **Figure 7. Predicted nitrite profiles from 'core' coastal MLR (green) and offshore MLR (blue). Observed nitrite profiles**
581 **from PPS 2016 dataset (deep pink).**

582

583

584

Biogeosciences

Discussions

EGU
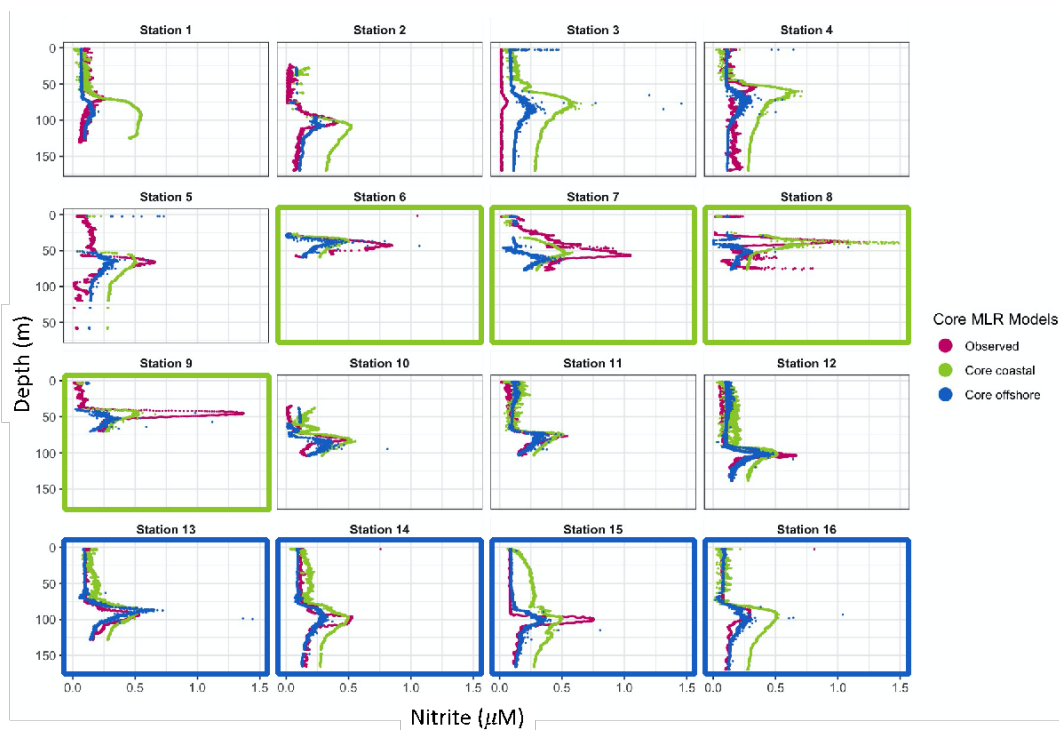
4 Discussion

4.1 Vertical structure of nitrite accumulation

The same vertical sequence of water column features was seen at all ETNP stations, with the chlorophyll maximum lying above the ammonium maximum lying above the depth of the nitrite maxima at the top of the nitracline. These consistent spatial relationships between water column features suggest that there is a specific set of environmental conditions and biological agents that lead to the accumulation of nitrite. Linear regressions between depth of the nitrite maxima and the depth of other key water column features indeed showed strong correlations. Previous work has noted the connection of the depth of the nitrite maxima with the nitracline (Dore and Karl, 1996; Herbland and Voituriez, 1979; Lomas and Lipschultz, 2006; Meeder et al., 2012; Shiozaki et al., 2016; Vaccaro and Ryther, 1960) and with the chlorophyll maximum (Collos, 1998; French et al., 1983; Kiefer et al., 1976; Meeder et al., 2012), showing that these relationships are shared across multiple oceanic regimes. The environmental feature that correlated most strongly with the depth of the nitrite maximum in our dataset was the top of the nitracline, with the depth of the chlorophyll maximum, the depth of the ammonium maximum, the depth of 1% PAR and the top of the oxycline also having strong correlations, as illustrated by regression analysis (Fig. 3).

The strong covariance between multiple features provides some insight into the mechanisms that link the depth of the nitrite maximum to the environment. Nitrite-cycling microbes respond to the differences in environmental conditions above and below the nitrite maximum. In oligotrophic waters, such as those in the offshore ETNP, uptake of nutrients by phytoplankton maintains low levels of DIN in the upper euphotic zone as physical resupply is low. As light decreases with depth in the water column, active phytoplankton growth is diminished and ammonium and labile dissolved organic nitrogen are released due to grazing and decomposition, providing the low-light, ammonium and reduced organic N conditions suitable for ammonia oxidation. Nitrite oxidizers utilize nitrite produced predominantly from ammonia oxidation to return nitrate to the system. Above the PNM, where light is available, there is enhanced potential for nitrite uptake by phytoplankton and nitrite does not accumulate. Below the PNM, there is diminished supply of ammonium and nitrite oxidizers continue to consume low levels of nitrite produced through ammonia oxidation. At the depth of the nitrite maximum, production terms outweigh both spatially segregated loss terms - nitrite uptake and nitrite oxidation.

The production of nitrite at the PNM is linked to the vertical sequential structuring of the upper water column qualities and is both directly and indirectly dependent on phytoplankton activity. It is directly related via the potential for phytoplankton to release nitrite under varying nitrate supply and light conditions, and indirectly through ammonium supply provided to the ammonia-oxidizing community. Interestingly, the sequence of events that structures the nitracline at the base of the euphotic zone (nitrate and light availability -> uptake of nitrate and phytoplankton growth -> formation of the nitracline and oxycline = release of ammonium (and nitrite) -> oxidation of ammonium by nitrifiers) is ordered similarly to the strength of the linear relationships with depth of the nitrite maximum (top of nitracline > %PAR > chlorophyll/ oxycline > ammonium peak depth). The physical processes that change light and mixing environments initiate the conditions under which phytoplankton and nitrifiers establish their contributions to

620 the PNM over time. The importance of the time component may help explain why there is variation in the strength of

621 correlation between instantaneous environmental measurements and a PNM structure that may have been forming

622 over weeks. Under more dynamic conditions (e.g, coastal upwelling), our observations are more likely to capture a

623 larger range in scenarios, from initial upwelling to cessation of upwelling, making correlations between depth of the

624 nitrite maximum and water column features weaker.

625 4.2 Concentration of the nitrite maximum

626 While the depth of the nitrite maximum is predictable based on features of the water column, the concentration of the

627 nitrite maximum was more challenging to predict. In regressions of water column features against the concentration

628 of the nitrite maximum, only the amount of nitrate at the nitrite maximum, the Brunt-Väisälä frequency and the amount

629 of oxygen at the nitrite maximum had moderate linear relationships (R^2=0.5, $p < 0.01$, $R^2 = 0.4$, $p = 0.016$, $R^2 = 0.29$,

630 $p = 0.019$), while the R^2 values for the other regressions were smaller ($R^2 < 0.25$) (Fig. 2). The connection between the

631 nitrite maximum and nitrate concentration may reflect the sequence of events that structures the water column and

632 forms the nitracline (described above). The presence of increased amounts of nitrate at the depth of larger nitrite

633 maxima suggests that the phytoplankton have yet to deplete nitrate completely, and a large nitrite maximum is

634 developing during active phytoplankton nitrate uptake at early bloom formation (Collos, 1982; Meeder et al., 2012).

635 At a station with a large nitrite maximum, there are also higher concentrations of nitrate at the chlorophyll maximum,

636 although the chlorophyll maximum may still be small (ie. early bloom). During this time, ammonium production from

637 degrading and grazed phytoplankton as well as ammonia oxidation to nitrite may co-occur. Under these early bloom

638 conditions there is potential to accumulate more nitrite due to increased rates of phytoplankton nitrate reduction, high

639 rates of ammonia oxidation, and/or decrease in loss terms. Controls on the nitrate reduction rate, and the potential for

640 ammonium competition interactions between phytoplankton and ammonia oxidizers at nitrate replete depths will be

641 discussed in relation to nitrite cycling rates.

642 The linear correlation between the larger nitrite maxima and stronger density gradients (higher Brunt-Väisälä values)

643 suggests that decreased loss of nitrite via mixing could contribute to larger accumulation of nitrite at the maximum.

644 However, degradation of the nitrite maximum by mixing would only move existing nitrite away from the peak depth,

645 not remove it entirely from the water column.

646 We took two further approaches to understand the correlative disconnect between environmental conditions and nitrite

647 maxima, 1) polynomial multiple regression analyses which allow multiple variables to co-explain the depth and

648 concentration of the nitrite maxima, and 2) making direct measurements of the microbial processes that

649 mechanistically link environmental conditions to the nitrogen transformation rates leading to nitrite accumulation.

650 4.3 Predicting nitrite profiles from environmental dataset

651 The lack of strong linear correlation between nitrite maxima and any single feature may indicate that multiple

652 conditions need to be met to produce large accumulations of nitrite. For example, other work has shown the largest

653   seasonal nitrite maxima occur at the onset of the deep chlorophyll maximum, where multiple conditions are met - light

654   is available and nitrate concentrations are still high (Mackey et al., 2011; Meeder et al., 2012).

655   Allowing for multiple environmental conditions to contribute, the 'full' multilinear regression models are qualitatively

656   able to capture the peak shape of the PNM feature using the variables provided, yet are unable to fully explain nitrite

657   concentration (Fig. 6). For example, the all-station 'full' model explained 66% of the overall variance in nitrite

658   concentration, and the mean error in nitrite maxima predictions was 740 nM with a large range in errors across stations

659   (-0.84 to 15.28 μM) (Table S4). This is not surprising, since environmental conditions vary across the ETNP,

660   especially between coastal and offshore stations. The coastal and offshore nitrite maxima were typically found at

661   similar densities (~24.1 kg m^{-3} coastal, ~24.3 kg m^{-3} offshore), but at coastal stations the average depth of the nitrite

662   maxima was 43 m shallower, the average nitrate concentration was 3x higher, the average chlorophyll concentration

663   was 3x higher, average light was 3x higher, oxygen was 25% higher and ammonium concentrations were also higher

664   (Table S2). This suggests that the nitrite maxima at coastal and offshore type stations may be innately different, and

665   possibly controlled by different mechanisms. Taking subsets of station data to make separate coastal and offshore

666   'full' models allowed for better explanatory power compared to grouping all of the stations together in a single MLR

667   model (Fig. S7). Model optimization selected different sets of variables to explain the nitrite concentrations in each

668   model, but nitrate was critical across all three models, aligning with results from the simple linear regression analyses,

669   where nitrate is important for explaining both depth of the nitrite maximum and the concentration of the nitrite

670   maximum. While the maximum nitrite concentration was not predicted well by these models, the mean error for the

671   depth of the Nitrite maximum was less than 4 m for all three 'full' models. However, the predicted depth of the Nitrite

672   maximum at individual stations could be more significantly erroneous (Table S4).

673   The 'core' models limited variables to those that had strong single linear regressions with depth and concentration of

674   the nitrite maxima, and both the coastal and offshore models explained similar amounts of the total variance in nitrite

675   concentration in their respective regions. Even though both models explained relatively similar amounts of variation

676   in nitrite concentration and used the same limited suite of variables, different coefficients led to differing predicted

677   nitrite profiles across stations (Fig. 7, Table 2). In the coastal region, the primary model components included nitrate

678   and light, two environmental conditions that are related to physical initiation of bloom conditions. The offshore model

679   shifts importance slightly towards a stronger chlorophyll component and reduces the importance of light.

680   The nitrate variables were involved in explaining similar amounts of the nitrite variance in both models (coastal and

681   offshore, 40.8% and 38.8%). Nitrate as a single variable also explained a similar portion of the total model variance

682   in both the coastal and offshore models (12.2%, 10.2% respectively). The coefficients for nitrate variables have the

683   same sign in both models, with nitrate having a negative coefficient and the two nitrate interaction terms having

684   positive coefficients. Overall, the negative nitrate coefficients act to decrease predicted nitrite below the nitrite maxima

685   where nitrate increases towards ~25 μM. The slightly more negative coefficient in the coastal model is counteracted

686   by the slightly higher concentrations of nitrate seen at coastal nitrite maxima. The oxygen and pPAR coefficients for

687   both models are also negative, and act to decrease predicted nitrite at the depths above the nitrite maximum. The

688   interaction terms containing nitrate in both models have positive coefficient values, adding nitrite to depths near the

689 PNM where nitrate, oxygen and chlorophyll are all present together. In both 'core' models, the interaction term
690 between nitrate and chlorophyll is an important variable (>10% R^2 in both). This suggests that nitrite accumulation
691 occurs at depths where chlorophyll, nitrate and oxygen co-exist, corroborating the findings from that linear regression
692 analyses, that the depth of the chlorophyll maxima, nitracline top and oxycline top are individually important in
693 determining the depth of the nitrite maximum.

694 The chlorophyll variables are the only coefficients that differ in sign between the two models, with the coastal
695 chlorophyll coefficient being negative and the offshore chlorophyll coefficient being positive. The quadratic term for
696 chlorophyll has a negative sign for both models, meaning the presence of a chlorophyll maximum decreases nitrite
697 predictions strongly just above the nitrite maximum (perhaps driven by nitrite uptake) and shifts the nitrite peak
698 towards the downslope of the chlorophyll maximum. The single chlorophyll term in the coastal model is also negative
699 and reduces nitrite predictions in direct proportion to the size of the chlorophyll peak. In contrast, the positive single
700 chlorophyll term in the offshore model means that, opposing the quadratic term, this variable adds nitrite at depths
701 across the chlorophyll maximum. Additionally, the single chlorophyll term in the offshore model is much larger in
702 absolute magnitude than the coastal term, which likely explains the poor performance of the offshore core model at
703 coastal stations where chlorophyll concentrations are often larger (Fig. 7). The smaller chlorophyll coefficients used
704 to model nitrite maxima at coastal stations make the model less sensitive to large changes in chlorophyll, while the
705 larger offshore coefficient suggests that small changes in chlorophyll offshore have more influence over the resulting
706 nitrite predictions.

707 **4.4 Rates of Nitrite Cycling**

708 Strong single variable correlations with depth of the nitrite maxima and mild correlations with concentration of nitrite
709 at the nitrite maxima (with supportive findings from the MLR analyses), suggest that while the PNM feature is
710 consistently limited to specific depths, the concentration of the nitrite maxima may be modulated by more nuanced
711 environmental timings and microbial physiologies. The two main mechanistic explanations for nitrite production at
712 the PNM involve the microbial physiology of phytoplankton and nitrifying bacteria/archaea. The overlapping habitats
713 and competition for DIN resources requires that we consider both microbial groups in our understanding of PNM
714 formation (Lomas and Lipschultz, 2006; Mackey et al., 2011; Smith et al., 2014; Wan et al., 2021, 2018; Zakem et
715 al., 2018). This dataset is particularly unique because we have directly measured four major nitrite cycling rates from
716 the same source water, allowing comparison of relative rates of each process within a community and enabling the
717 calculation of net rates of nitrite production around the PNM feature. Our expectation at the beginning of this study
718 was that higher rates of nitrite production, or net nitrite production, would correspond to larger accumulation of nitrite.
719 Our findings, however, revealed a more complex pattern where the instantaneous rates of gross or net nitrite
720 production did not reflect the amount of observed accumulated nitrite.

721 The spatial distribution of measured rates through the water column showed peaks in each process near the PNM,
722 but with slight variation in where the rate maxima fell relative to the nitrite maxima. The highest phytoplankton activity
723 was located just above the PNM peak, while nitrification rates were highest near the PNM peak and distributed in a

724   peak shape, a distribution seen in other nearby systems (Beman et al., 2012; Santoro et al., 2013). Although the

725   aggregated data from the region showed these spatial segregations by microbial group, this was not always observed

726   at an individual station. The highest rates of nitrification may be slightly skewed towards the lower slope of the PNM,

727   but the depth of the nitrite maximum at many stations was determined from discrete measurements taken at ~10 m

728   resolution, so it is possible that the real maxima occurred between sampled depths. The PPS data allowed much more

729   precise determination of the depth and peak size, although rate measurements were still limited to lower resolution

730   sampling.

731   The vertical distribution of nitrification has been theorized to be controlled by light inhibition, restricting nitrification

732   to depths at the base of the euphotic zone (Olson, 1981). However, active nitrification has been observed in the sunlit

733   surface ocean (Shiozaki et al., 2016; Ward, 2005; Ward et al., 1989), leading to new theories suggesting that ammonia

734   oxidation is restricted to near the PNM not only because of inhibition at high light levels, but because ammonium or

735   nitrate availability shifts the competitive balance for ammonium acquisition away from phytoplankton and towards

736   ammonia oxidizers (Smith et al., 2014; Wan et al., 2018; Xu et al., 2019). In this dataset, we did measure nitrification

737   rates >2 nM day^{-1} at light levels of 25-30% surface PAR at coastal stations, although there was a clear enhancement

738   of nitrification rates at light levels below 5% surface PAR. Although linear regressions of ammonia oxidation rate

739   didn't show a strong correlation with the nitrite maxima or depth of the nitrite maxima, there was a relationship

740   between ammonia oxidation and both nitrate and light (Fig. 8). Similar to the data compiled in Wan et al. (2018), the

741   highest ammonia oxidation rates were restricted to depths with higher nitrate concentrations and lower light levels.

742   However, even when constraining the ammonia oxidation rate data to where there is both low light and higher nitrate

743   concentrations, measurements spanned the entire range of rates from 0-85 nM day^{-1}, indicating that the conditions

744   controlling the depth of the rate maxima do not guarantee high rates, but simply facilitate the possibility of high rates.

745 **Figure 8. Relationship between nitrite cycling rates and percent surface PAR (a) and nitrate concentration (b).**
746 **Phytoplankton processes are in green and nitrifier processes are in orange. Nitrite consumption processes are x shapes**
747 **and production processes are filled circles.**
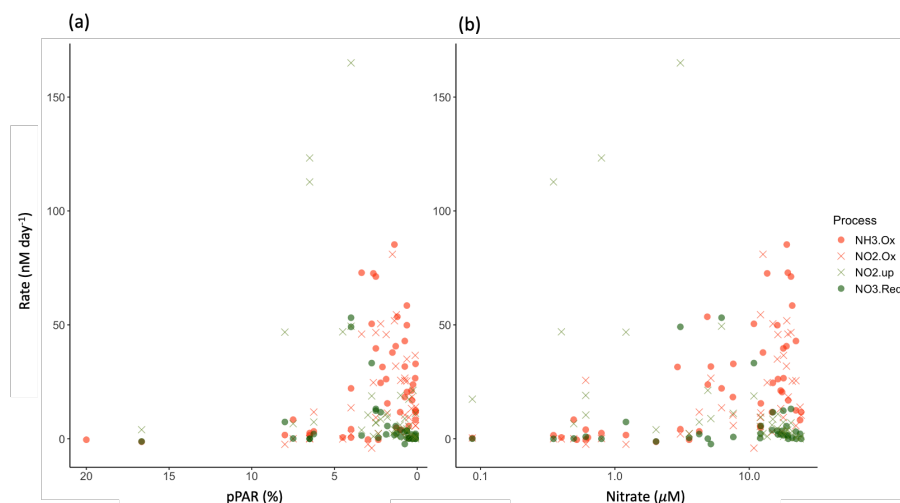
748

749 The individual rate measurements were not correlated with the amount of nitrite accumulated in the water column at
750 a given depth (Fig. S4). Neither were the net rates (NetNit, NetPhy, NetNO2) able to explain observed nitrite
751 concentrations. Although the vertical pattern in net nitrite production rates (NetNO2) showed a peak shape that was
752 qualitatively similar to nitrite concentration, there was no linear relationship between NetNO2 and nitrite
753 concentration (Fig. 4h, Fig. S4), suggesting that instantaneous in situ rate measurements are not able to capture time-
754 integrated nitrite accumulation in the PNM. Modeling efforts that are able to integrate fluctuations in environmental
755 influence on microbial rates over longer time scales may be more able to explain observed nitrite concentrations.

756 Nitrification rates were similar in magnitude between coastal and offshore stations (Table S2), with the major
757 differences in rates measurements between coastal and offshore stations found in the phytoplankton processes (nitrate
758 reduction and nitrite uptake). The highest rates of phytoplankton activity were at coastal stations and occurred
759 primarily above the depth of the nitrite maximum. The distribution of measured activity lends support to the hypothesis
760 that phytoplankton may outcompete nitrifiers for DIN sources above the nitrite maxima (Wan et al., 2018; Zakem et
761 al., 2018). This proposed mechanism accounts for the correlations seen between lower light levels and higher ammonia
762 oxidation because the top of the nitracline itself is a physical demarcation of the depth where phytoplankton co-
763 requirements for light and nitrate are met. Previous work has also shown that the presence of nitrate can inhibit nitrite
764 uptake by phytoplankton through competitive interactions (Eppley and Coatsworth, 1968; Raimbault, 1986) (Fig.8b).
765 This mechanism may provide a way to connect the presence of nitrate with a larger PNM that relies on prevention of
766 nitrite loss, rather than an increase in nitrite production.

767 An additional loss term that could influence the size of the observed nitrite peak may be diffusion, moving nitrite away
768 (both up and down) from the depth of maximal net nitrite production. The coastal stations were grouped based on the

769 presence of shallow nitraclines and shallow chlorophyll maxima depths, as well as larger chlorophyll maxima and

770 nitrite maxima. In addition to these commonalities, the coastal stations also had the steepest density gradients near the

771 observed larger PNM, making Brunt-Väisälä (BV) frequency correlate with the nitrite maxima in this dataset

772 (p=0.005) (Fig. 2l). The strong density gradients at the coastal stations (6,7,8,9) would inhibit mixing, potentially

773 allowing for larger concentrations of nitrite to accumulate where gradients are steepest. This lack of diffusive loss at

774 coastal stations could partially explain why ammonia oxidation rates can remain similar between coastal and offshore

775 stations (25.8 ± 3.6 vs 21.3 ± 3.3 nM day^{-1}), yet result in higher accumulated nitrite at an coastal PNM.

4.5 Different time scales inherent to observational patterns

777 Environmental features may not explain the concentration of the nitrite maxima because of a time lag between

778 environmental conditions measured at a station and the response of the microbial community, and the length of time

779 needed to produce a PNM. Previous work has shown that a seasonal PNM can develop over 6 days in the Gulf of

780 Aqaba (Mackey et al., 2011). In our study, a large range was observed in net production rates (~0-86.9 nM day^{-1}),

781 leading to the potential for a PNM to develop in less than a day at some locations, and months at other stations.

782 However, an imbalance in nitrite production and consumption merely tells you whether nitrite is currently increasing

783 or decreasing, not whether the instantaneously observed nitrite concentration should be high or low. Calculations from

784 rate estimates and isotope data suggest 20-50 day residence times for nitrite in the Arabian Sea PNM (Buchwald and

785 Casciotti, 2013). Ammonia oxidation measurements from the California Current System suggested an 18-470 day

786 residence time for offshore stations, and 40 day residence time for a coastal station (see full table in Santoro et al.

787 2013). Our residence time calculations, on the order of days to months, are consistent with these estimates of PNM

788 residence times (Fig. S6). The high variability in accumulation times across sample locations makes it less likely that

789 snapshots of rates and environmental conditions would be representative of conditions for a PNM developing over

790 longer timescales.

4.6 Spatiotemporal controls on the nitrite maximum

792 Previous work investigating the onset of the classic PNM has shown that nitrite concentrations are highest at the

793 beginning of seasonal stratification when phytoplankton begin to bloom, suggesting that phytoplankton help provide

794 the necessary conditions for nitrite accumulation (Al-Qutob et al., 2002; Mackey et al., 2011; Meeder et al., 2012;

795 Vaccaro and Ryther, 1960). In Mackey et al. (2011), the onset of stratification initiates a phytoplankton bloom that

796 begins to deplete surface nitrate and releases ammonia via phytoplankton degradation and zooplankton grazing. An

797 accumulation of ammonium forms just below the chlorophyll maximum, which is subsequently followed by an

798 accumulation of nitrite just below the ammonium peak. This continued stratification pattern supports the persistence

799 of the emergent PNM feature, though the size of the nitrite maximum declines over the duration of the stratification

800 period. The correlation between coastal upwelling and higher nitrite accumulation in the ETNP PNM may be

801 controlled by similar mechanisms as the high nitrite accumulation at the onset of seasonal stratification in other

802 regions. Instead of a strongly seasonal onset of stratification, the ETNP stratification persists year-round but is

803 modulated by upwelling along the coast.

804   At coastal stations in 2016, we saw higher average concentrations of nitrate (16μM) at the depth of the nitrite maxima

805   due to upwelling conditions, while average nitrate concentrations at offshore nitrite maxima were lower (5.9 μM). The

806   positive correlation of nitrate concentration at the PNM peak with the concentration of the nitrite maximum (R^2=0.5,

807   p=0.01) suggests that upwelling nitrate is critical for larger nitrite maxima. The correlation found in the MLR analysis

808   between the chlorophyll-nitrate interaction term and the nitrite maxima supports the idea that higher nitrite

809   accumulation requires the presence of higher levels of nitrate within the chlorophyll bloom. High variation in the

810   correlation of nitrite maxima with chlorophyll, ammonium and nitrate may be due to how recently the chlorophyll

811   bloom was initiated (has the bloom had time to draw down available nitrate?). However, these patterns do not identify

812   whether the presence of nitrate drives nitrite production from phytoplankton directly, or indirectly by stimulating

813   ammonia oxidation, or is a proxy for a more stratified water column.

814   Sequential decomposition of particulate organic nitrogen (PON) produces ammonium, then nitrite, and nitrate over

815   time, and matches the spatial ordering of these species with depth in the water column (Meeder et al. 2012). In a

816   stratified water column, the vertical transport of material may be slow enough to allow for a similar temporal

817   degradation pattern to emerge across the pycnocline. The sequence is initiated by the blooming of phytoplankton,

818   which is restricted to surface depths with adequate light and nitrate. In a coastal upwelling regime, the stratified water

819   column is pushed up towards the surface, and this degradation sequence is modified by enhanced source PON from

820   larger chlorophyll blooms. Larger pools of chlorophyll lead to larger ammonium and nitrite accumulation. Based on

821   the magnitude of net nitrite production attributed to phytoplankton vs. nitrifiers, nitrifiers appear to have a larger

822   potential for net nitrite production at ETNP PNMs. The association of nitrification rates with increasing nitrate

823   concentration, which is not a required substrate for nitrification, indicates an indirect connection with phytoplankton

824   activity which is typically dependent on nitrate availability. We suggest that changes in light and nitrate availability

825   initiate a cascade of microbial processes that degrade phytoplankton-based PON into DON, providing a substrate for

826   ammonia oxidation, and resulting in PNM formation.

827   **Figure 9. Schematic of nitrite cycling processes and relative DIN pools near the PNM feature. Panel (a) depicts the**
828   **offshore conditions and panel (b) depicts early upwelling conditions that lead to bloom initiation.**
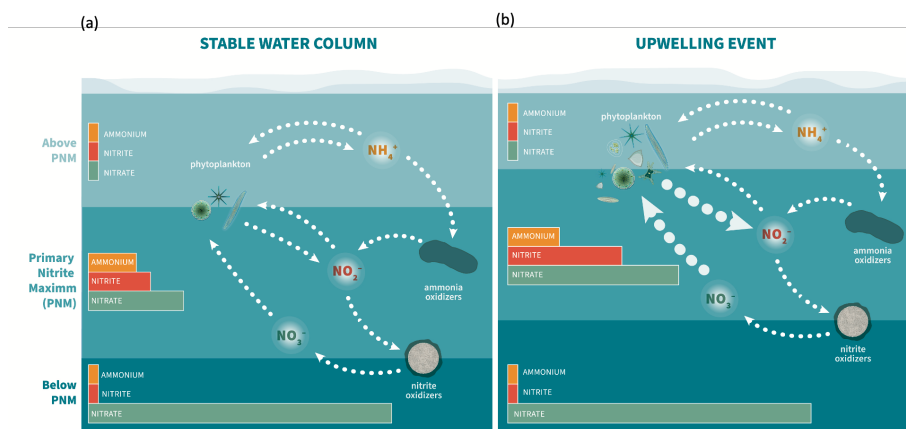

829

830   Figure 9 places the findings in the current study in the context of the sequential physical and biological processes

831   controlling the PNM feature in the ETNP. The schematic depicts a typical offshore PNM observed during a stratified,

832   stable water column (Fig. 9a), in contrast to that observed during the onset of upwelling (Fig. 9b). In each case, the

833   surface ocean is split into 3 layers: above, within, and below the PNM, with the PNM sitting near the top of the

834   nitracline. Phytoplankton control the availability and supply of DIN above the PNM, where high light allows for

835   complete drawdown of DIN. In the stable water column (Fig. 9a), phytoplankton are present in a chlorophyll maximum

836   that is small and stable just above the nitracline consisting of smaller eukaryotes and cyanobacteria (Legendre-Fixx,

837   2017). The chlorophyll maximum is small because there is no active upwelling, and the ambient nitrate at the

838   chlorophyll maximum has been depleted to low concentrations. Phytoplankton fail to access deeper nitrogen supplies

839   because light levels become inadequate at depth, so the chlorophyll maximum is balanced at the intersection of the

840   dual requirements for light and upwardly diffused nitrate. A small ammonium peak develops just below the

841   chlorophyll maximum, and just above the nitrite maximum, coming from phytoplankton decomposition processes

842   including grazer activity. The supply of ammonium is adequate to fuel an active nitrifier community in the PNM layer

843   and below, with average rates of ammonia oxidation and nitrite oxidation near 20 nM day^{-1}. The net imbalance in the

844   two steps of nitrification is small (few nM day^{-1}), contributing to the small yet stable accumulation of nitrite at the

845   PNM. Contributions of nitrite from phytoplankton are minimal because they have drawn down surface nitrate and are

846   subsisting at the edge of a well-established deep nitracline. Although the water column is stably stratified, the Brunt-

847   Väisälä values are moderate.

848   During an upwelling event (Fig. 9b), an influx of nitrate-rich water into the euphotic zone initiates a phytoplankton

849   bloom. We see evidence of early upwelling at coastal stations where nitrate concentrations at the chlorophyll

850   maximum are not completely depleted (average 5.2±3.6 μM), while nitrate at offshore station chlorophyll maxima are

851   lower (average 0.6±0.4 μM). With phytoplankton growth fueled by new nitrate, the ammonium concentration begins

852   to increase via degradation and grazing, providing substrate for ammonia oxidizers. Rate measurements show a small

853   increase in average ammonia oxidation rate at coastal stations compared to offshore stations (25.8±3.6 vs. 21.3±3.3

854   nM day^{-1}, respectively). At some coastal stations, a more significant change in the concentration of the nitrite

855   maximum may come from increased phytoplankton nitrite release. Nitrate reduction rates larger than ammonia

856   oxidation rates (>30 nM day^{-1}) were measured sporadically at stations near the coast. Previous work has documented

857   up to ~10% of nitrate uptake can be released as nitrite in laboratory culture experiments, suggesting that locations with

858   high nitrate uptake and active nitrate reduction have the potential for more nitrite release from phytoplankton (Collos,

859   1998). Additionally, the physical upwelling of deep water compresses density layers in the euphotic zone leading to

860   higher Brunt-Väisälä values and lower potential for nitrite diffusion away from the site of production, helping to

861   explain larger nitrite maxima occurring at upwelling sites.

862   **5 Conclusions**

863   This study used both high resolution environmental data and direct rate measurements of nitrite cycling processes to

864   explore the factors contributing to PNM formation in ETNP. At our sites, there was a distinct and predictable depth

865 where nitrite accumulated in a peak-shaped PNM feature. Linear regression and multivariate regression analysis with
866 environmental data showed that the top of the nitracline and the top of the oxycline are two major indicators of the
867 depth of the nitrite maximum. Rate data also showed distinct peaks in activity that corresponded well with the mean
868 PNM isopycnal for the region. Nitrifier processes dominated nitrite cycling at and below the PNM, while
869 phytoplankton processes were typically restricted to depths above the PNM. Ammonia oxidation was the dominant
870 nitrite production process at most depths and stations. We report a handful of high nitrate reduction rates (>20 nM
871 day^{-1}) from coastal stations with higher chlorophyll and nitrate concentrations at the PNM, which suggest there are
872 opportunities for phytoplankton to play a larger role in nitrite production at the PNM under these conditions. However,
873 even where nitrite production from phytoplankton remains low, we suggest a sequential and competitive dependence
874 of ammonia oxidation rates on phytoplankton processes. The importance of co-occurring environmental conditions
875 and timing lag of microbial interactions should be considered in further work on what determines the formation of
876 large nitrite maxima. For example, both nitrate and light availability may work together to control net nitrite production
877 through sequential processes beginning with upwelling events. Microbial physiological responses remain important
878 in connecting rates of activity to dynamic environmental conditions.

879 With nitrite production in the PNM predominantly linked to ammonia oxidation, this has potential implications for
880 production of nitrous oxide in the upper water column of the ETNP. The ETNP is known to be an important source
881 for atmospheric nitrous oxide (Babbin et al., 2020; Tian et al., 2020), with high accumulations of nitrous oxide in the
882 near surface (Kelly et al., 2021; Monreal et al., 2022). Nitrous oxide production in the near-surface maximum has
883 been linked to a combination of hybrid production from AOA, and bacterial denitrification (Kelly et al., 2021; Monreal
884 et al., 2022; Trimmer et al., 2016). Conditions that favor enhanced ammonia oxidation could thus also promote
885 enhanced nitrous oxide production and emissions thereby forming a link between stimulation of high primary
886 productivity and high rates of nitrous oxide production and emission.

References

888 Al-Qutob, M., Häse, C., Tilzer, M. M., and Lazar, B.: Phytoplankton drives nitrite dynamics in the Gulf of Aqaba,
889 Red Sea, 239, 233–239, https://doi.org/10.3354/meps239233, 2002.

890 Babbin, A. R., Boles, E. L., Mühle, J., and Weiss, R. F.: On the natural spatio-temporal heterogeneity of South
891 Pacific nitrous oxide, 11, 1–9, https://doi.org/10.1038/s41467-020-17509-6, 2020.

892 Beman, J. M., Popp, B. N., and Francis, C. A.: Molecular and biogeochemical evidence for ammonia oxidation by
893 marine Crenarchaeota in the Gulf of California, 2, 429–441, https://doi.org/10.1038/ismej.2007.118, 2008.

894 Beman, J. M., Popp, B. N., and Alford, S. E.: Quantification of ammonia oxidation rates and ammonia-oxidizing
895 archaea and bacteria at high resolution in the Gulf of California and eastern tropical North Pacific Ocean, 57, 711–
896 726, https://doi.org/10.4319/lo.2012.57.3.0711, 2012.

897 Beman, J. M., Shih, J. L., and Popp, B. N.: Nitrite oxidation in the upper water column and oxygen minimum zone
898 of the eastern tropical North Pacific Ocean, 7, 2192–2205, https://doi.org/10.1038/ismej.2013.96, 2013.

Biogeosciences
Discussions

899   Böhlke, J. K., Mroczkowski, S. J., and Coplen, T. B.: Oxygen isotopes in nitrate: new reference materials for [18] O: [17]
900   O: [16] O measurements and observations on nitrate-water equilibration: Reference materials for O-isotopes in nitrate,
901   Rapid Commun. Mass Spectrom., 17, 1835–1846, https://doi.org/10.1002/rcm.1123, 2003.

902   Brandhorst, W.: Nitrite Accumulation in the North-East Tropical Pacific, Nature, 182, 679–679,
903   https://doi.org/10.1038/182679a0, 1958.

904   Bronk, D. A., Glibert, P. M., and Ward, B. B.: Nitrogen Uptake, Dissolved Organic Nitrogen Release, and New
905   Production, Science, 265, 1843–1846, https://doi.org/10.1126/science.265.5180.1843, 1994.

906   Buchwald, C. and Casciotti, K. L.: Isotopic ratios of nitrite as tracers of the sources and age of oceanic nitrite, 6,
907   308–313, https://doi.org/10.1038/NGEO1745, 2013.

908   Burlacot, A., Richaud, P., Gosset, A., Li-Beisson, Y., and Peltier, G.: Algal photosynthesis converts nitric oxide into
909   nitrous oxide, Proc Natl Acad Sci USA, 117, 2704–2709, https://doi.org/10.1073/pnas.1915276117, 2020.

910   Carlucci, A. F., Hartwig, E. O., and Bowes, P. M.: Biological production of nitrite in seawater, 7, 161–166,
911   https://doi.org/10.1007/BF00354921, 1970.

912   Casciotti, K. L., Böhlke, J. K., McIlvin, M. R., Mroczkowski, S. J., and Hannon, J. E.: Oxygen isotopes in nitrite:
913   analysis, calibration, and equilibration, 79, 2427–2436, https://doi.org/10.1021/ac061598h, 2007.

914   Cline, J. D. and Richards, F. A.: Oxygen deficient conditions and nitrate reduction in the eastern tropical North
915   Pacific Ocean, 17, 885–900, https://doi.org/10.4319/lo.1972.17.6.0885, 1972.

916   Codispoti, L. A., Friederich, G. E., Murray, J. W., and Sakamoto, C. M.: Chemical variability in the Black Sea:
917   implications of continuous vertical profiles that penetrated the oxic/anoxic interface, Deep Sea Research Part A.
918   Oceanographic Research Papers, 38, S691–S710, https://doi.org/10.1016/S0198-0149(10)80004-4, 1991.

919   Collos, Y.: Transient situations in nitrate assimilation by marine diatoms. 2. Changes in nitrate and nitrite following
920   a nitrate perturbation, 27, 528–535, https://doi.org/10.1.1.597.3625, 1982.

921   Collos, Y.: Nitrate uptake, nitrite release and uptake, and new production estimates, 171, 293–301, 1998.

922   Cornec, M., Claustre, H., Mignot, A., Guidi, L., Lacour, L., Poteau, A., D'Ortenzio, F., Gentili, B., and Schmechtig,
923   C.: Deep Chlorophyll Maxima in the Global Ocean: Occurrences, Drivers and Characteristics, Global Biogeochem
924   Cycles, 35, https://doi.org/10.1029/2020GB006759, 2021.

925   Dore, J. E. and Karl, D. M.: Nitrification in the euphotic zone as a source for nitrite, nitrate, and nitrous oxide at
926   Station ALOHA, 41, 1619–1628, https://doi.org/10.4319/lo.1996.41.8.1619, 1996.

927   Dugdale, R. and Goering, J.: Uptake of new and regenerated forms of nitrogen in primary productivity, 12, 196–206,
928   1967.

929   Dugdale, R. and Wilkerson, F.: The use of 15N to measure nitrogen uptake in eutrophic oceans; experimental
930   considerations1, 2, 31, 673–689, 1986.

931   Eppley, R. W. and Coatsworth, J. L.: Uptake of nitrate and nitrite by Ditylum Brightwelli - Kinetics and
932   mechanisms, 4, 151–156, https://doi.org/10.1111/j.1529-8817.1968.tb04689.x, 1968.

933   Francis, C. A., Roberts, K. J., Beman, J. M., Santoro, A. E., and Oakley, B. B.: Ubiquity and diversity of ammonia-
934   oxidizing archaea in water columns and sediments of the ocean, 102, 14683–14688,
935   https://doi.org/10.1073/pnas.0506625102, 2005.

936   Francis, C. A., Beman, J. M., and Kuypers, M. M. M.: New processes and players in the nitrogen cycle: the
937   microbial ecology of anaerobic and archaeal ammonia oxidation, 1, 19–27, https://doi.org/10.1038/ismej.2007.8,
938   2007.

939   French, D. P., Furnas, M. J., and Smayda, T. J.: Diel changes in nitrite concentration in the chlorophyll maximum in
940   the Gulf of Mexico, 30, 707–722, https://doi.org/10.1073/pnas.0506625102, 1983.

941   Füssel, J., Lam, P., Lavik, G., Jensen, M. M., Holtappels, M., Günter, M., and Kuypers, M. M.: Nitrite oxidation in
942   the Namibian oxygen minimum zone, 6, 1200–1209, https://doi.org/10.1038/ismej.2011.178, 2012.

943   Glibert, P. M., Middelburg, J. J., McClelland, J. W., and Jake Vander Zanden, M.: Stable isotope tracers: Enriching
944   our perspectives and questions on sources, fates, rates, and pathways of major elements in aquatic systems, Limnol
945   Oceanogr, 64, 950–981, https://doi.org/10.1002/lno.11087, 2019.

946   GLODAP, V.: GLODAP V2, V2.

947   Granger, J. and Sigman, D. M.: Removal of nitrite with sulfamic acid for nitrate N and O isotope analysis with the
948   denitrifier method, 23, 3753–3762, https://doi.org/10.1002/rcm.4307, 2009.

949   Grömping, U.: Relative Importance for Linear Regression in R: The Package relaimpo, 17, 1–27, 2006.

950   Gruber, N.: The marine nitrogen cycle: overview and challenges, 2, 1–50, https://doi.org/10.1038/nature06592,
951   2008.

952   Guerrero, M. A. and Jones, R. D.: Photoinhibition of marine nitrifying bacteria. I. Wavelength-dependent response,
953   141, 183–192, https://doi.org/10.3354/meps141183, 1996.

954   Herbland, A. and Voituriez, B.: Hydrological structure analysis for estimating the primary production in the tropical
955   Atlantic Ocean, 37, 16, 1979.

956   Holligan, P. M., Balch, W. M., and Yentsch, C. M.: The significance of subsurface chlorophyll, nitrite and
957   ammonium maxima in relation to nitrogen for phytoplankton growth in stratified waters of the Gulf of Maine, 42,
958   1051–1073, https://doi.org/10.1357/002224084788520747, 1984.

959   Holmes, R. M., Aminot, A., Kérouel, R., Hooker, B. A., and Peterson, B. J.: A simple and precise method for
960   measuring ammonium in marine and freshwater ecosystems, 56, 1801–1808, https://doi.org/10.1139/f99-128, 1999.

961   Horak, R. E. A., Qin, W., Bertagnolli, A. D., Nelson, A., Heal, K. R., Han, H., Heller, M., Schauer, A. J., Jeffrey, W.
962   H., Armbrust, E. V., Moffett, J. W., Ingalls, A. E., Stahl, D. A., and Devol, A. H.: Relative impacts of light,
963   temperature, and reactive oxygen on thaumarchaeal ammonia oxidation in the North Pacific Ocean, 63, 741–757,
964   https://doi.org/10.1002/lno.10665, 2018.

965   Kelly, C. L., Travis, N. M., Baya, P. A., and Casciotti, K. L.: Quantifying Nitrous Oxide Cycling Regimes in the
966   Eastern Tropical North Pacific Ocean With Isotopomer Analysis, Global Biogeochem Cycles, 35,
967   https://doi.org/10.1029/2020GB006637, 2021.

968   Kiefer, D., Olson, R., and Holm-Hansen, O.: Another look at the nitrite and chlorophyll maxima in the central North
969   Pacific, in: Deep Sea Research and Oceanographic Abstracts, 1199–1208, https://doi.org/10.1016/0011-
970   7471(76)90895-0, 1976.

971   Legendre-Fixx, M.: Drivers of phytoplankton community heterogeneity in the Eastern Tropical North Pacific,
972   Undergraduate Thesis, University of Washington, 2017.

973   Lomas, M. and Glibert, P.: Interactions between NH+ 4 and NO- 3 uptake and assimilation: comparison of diatoms
974   and dinoflagellates at several growth temperatures, 133, 541–551, https://doi.org/10.1007/s002270050494, 1999.

975 Lomas, M. W. and Glibert, P. M.: Comparisons of nitrate uptake, storage, and reduction in marine diatoms and
976 flagellates, 36, 903–913, https://doi.org/10.1046/j.1529-8817.2000.99029.x, 2000.

977 Lomas, M. W. and Lipschultz, F.: Forming the primary nitrite maximum: Nitrifiers or phytoplankton?, 51, 2453–
978 2467, https://doi.org/10.4319/lo.2006.51.5.2453, 2006.

979 Lücker, S., Wagner, M., Maixner, F., Pelletier, E., Koch, H., Vacherie, B., Rattei, T., Damsté, J. S. S., Spieck, E., Le
980 Paslier, D., and Daims, H.: A *Nitrospira* metagenome illuminates the physiology and evolution of globally
981 important nitrite-oxidizing bacteria, Proc. Natl. Acad. Sci. U.S.A., 107, 13479–13484,
982 https://doi.org/10.1073/pnas.1003860107, 2010.

983 Lücker, S., Nowka, B., Rattei, T., Spieck, E., and Daims, H.: The Genome of Nitrospina gracilis Illuminates the
984 Metabolism and Evolution of the Major Marine Nitrite Oxidizer, Front. Microbio., 4,
985 https://doi.org/10.3389/fmicb.2013.00027, 2013.

986 Mackey, K. R., Bristow, L., Parks, D. R., Altabet, M. A., Post, A. F., and Paytan, A.: The influence of light on
987 nitrogen cycling and the primary nitrite maximum in a seasonally stratified sea, 91, 545–560,
988 https://doi.org/10.1016/j.pocean.2011.09.001, 2011.

989 Martens-Habbena, W., Berube, P. M., Urakawa, H., de la Torre, J. R., and Stahl, D. A.: Ammonia oxidation kinetics
990 determine niche separation of nitrifying Archaea and Bacteria, Nature, 461, 976–979,
991 https://doi.org/10.1038/nature08465, 2009.

992 McIlvin, M. R. and Altabet, M. A.: Chemical conversion of nitrate and nitrite to nitrous oxide for nitrogen and
993 oxygen isotopic analysis in freshwater and seawater, 77, 5589–5595, https://doi.org/10.1021/ac050528s, 2005.

994 McIlvin, M. R. and Casciotti, K. L.: Technical updates to the bacterial method for nitrate isotopic analyses, 83,
995 1850–1856, https://doi.org/10.1021/ac1028984, 2011.

996 Meeder, E., Mackey, K. R., Paytan, A., Shaked, Y., Iluz, D., Stambler, N., Rivlin, T., Post, A. F., and Lazar, B.:
997 Nitrite dynamics in the open ocean-clues from seasonal and diurnal variations, 453,
998 https://doi.org/10.3354/meps09525, 2012.

999 Merbt, S. N., Stahl, D. A., Casamayor, E. O., Martí, E., Nicol, G. W., and Prosser, J. I.: Differential photoinhibition
1000 of bacterial and archaeal ammonia oxidation, 327, 41–46, https://doi.org/10.1111/j.1574-6968.2011.02457.x, 2012.

1001 Miller, T. L. based on F. code by A.: leaps: Regression Subset Selection, 2020.

1002 Mincer, T. J., Church, M. J., Taylor, L. T., Preston, C., Karl, D. M., and DeLong, E. F.: Quantitative distribution of
1003 presumptive archaeal and bacterial nitrifiers in Monterey Bay and the North Pacific Subtropical Gyre, 9, 1162–1175,
1004 https://doi.org/10.1111/j.1462-2920.2007.01239.x, 2007.

1005 Monreal, P. J., Kelly, C. L., Travis, N. M., and Casciotti, K. L.: Identifying the Sources and Drivers of Nitrous
1006 Oxide Accumulation in the Eddy-Influenced Eastern Tropical North Pacific Oxygen-Deficient Zone, Global
1007 Biogeochemical Cycles, 36, https://doi.org/10.1029/2022GB007310, 2022.

1008 Mulholland, M. R. and Lomas, M. W.: Nitrogen uptake and assimilation, 303–384, 2008.

1009 Olson, R. J.: Differential photoinhibition of marine nitrifying bacteria: a possible mechanism for the formation of the
1010 primary nitrite maximum, 39, 227–238, 1981.

1011 Peng, X., Fuchsman, C. A., Jayakumar, A., Oleynik, S., Martens-Habbena, W., Devol, A. H., and Ward, B. B.:
1012 Ammonia and nitrite oxidation in the Eastern Tropical North Pacific: AMMONIA AND NITRITE OXIDATION IN
1013 ETNP, 29, 2034–2049, https://doi.org/10.1002/2015GB005278, 2015.

1014   Plouviez, M., Shilton, A., Packer, M. A., and Guieysse, B.: Nitrous oxide emissions from microalgae: potential
1015   pathways and significance, J Appl Phycol, 31, 1–8, https://doi.org/10.1007/s10811-018-1531-1, 2019.

1016   Raimbault, P.: Effect of temperature on nitrite excretion by three marine diatoms during nitrate uptake, 92, 149–155,
1017   1986.

1018   Sakamoto, C. M., Friederich, G. E., and Codispoti, L. A.: MBARI procedures for automated nutrient analyses using
1019   a modified Alpkem Series 300 Rapid Flow Analyzer, 1990.

1020   Santoro, A., Sakamoto, C., Smith, J., Plant, J., Gehman, A., Worden, A., Johnson, K., Francis, C., and Casciotti, K.:
1021   Measurements of nitrite production in and around the primary nitrite maximum in the central California Current, 10,
1022   7395–7410, 2013.

1023   Santoro, A. E., Casciotti, K. L., and Francis, C. A.: Activity, abundance and diversity of nitrifying archaea and
1024   bacteria in the central California Current, 12, 1989–2006, 2010.

1025   Santoro, A. E., Buchwald, C., McIlvin, M. R., and Casciotti, K. L.: Isotopic signature of N2O produced by marine
1026   ammonia-oxidizing archaea, 333, 1282–1285, 2011.

1027   Schaefer, S. C. and Hollibaugh, J. T.: Temperature Decouples Ammonium and Nitrite Oxidation in Coastal Waters,
1028   51, 3157–3164, https://doi.org/10.1021/acs.est.6b03483, 2017.

1029   Schleper, C., Jurgens, G., and Jonuscheit, M.: Genomic studies of uncultivated archaea, Nat Rev Microbiol, 3, 479–
1030   488, https://doi.org/10.1038/nrmicro1159, 2005.

1031   Shiozaki, T., Ijichi, M., Isobe, K., Hashihama, F., Nakamura, K., Ehama, M., Hayashizaki, K., Takahashi, K.,
1032   Hamasaki, K., and Furuya, K.: Nitrification and its influence on biogeochemical cycles from the equatorial Pacific
1033   to the Arctic Ocean, 10, 2184, 2016.

1034   Sigman, D. M., Casciotti, K. L., Andreani, M., Barford, C., Galanter, M., and Böhlke, J. K.: A Bacterial Method for
1035   the Nitrogen Isotopic Analysis of Nitrate in Seawater and Freshwater, Anal. Chem., 73, 4145–4153,
1036   https://doi.org/10.1021/ac010088e, 2001.

1037   Smith, J. M., Chavez, F. P., and Francis, C. A.: Ammonium uptake by phytoplankton regulates nitrification in the
1038   sunlit ocean, 9, e108173, 2014.

1039   Strickland, J. D. and Parsons, T. R.: A practical handbook of seawater analysis, 1972.

1040   Tian, H., Xu, R., Canadell, J. G., Thompson, R. L., Winiwarter, W., Suntharalingam, P., Davidson, E. A., Ciais, P.,
1041   Jackson, R. B., Janssens-Maenhout, G., Prather, M. J., Regnier, P., Pan, N., Pan, S., Peters, G. P., Shi, H., Tubiello,
1042   F. N., Zaehle, S., Zhou, F., Arneth, A., Battaglia, G., Berthet, S., Bopp, L., Bouwman, A. F., Buitenhuis, E. T.,
1043   Chang, J., Chipperfield, M. P., Dangal, S. R. S., Dlugokencky, E., Elkins, J. W., Eyre, B. D., Fu, B., Hall, B., Ito, A.,
1044   Joos, F., Krummel, P. B., Landolfi, A., Laruelle, G. G., Lauerwald, R., Li, W., Lienert, S., Maavara, T., MacLeod,
1045   M., Millet, D. B., Olin, S., Patra, P. K., Prinn, R. G., Raymond, P. A., Ruiz, D. J., van der Werf, G. R., Vuichard, N.,
1046   Wang, J., Weiss, R. F., Wells, K. C., Wilson, C., Yang, J., and Yao, Y.: A comprehensive quantification of global
1047   nitrous oxide sources and sinks, Nature, 586, 248–256, https://doi.org/10.1038/s41586-020-2780-0, 2020.

1048   Trimmer, M., Chronopoulou, P.-M., Maanoja, S. T., Upstill-Goddard, R. C., Kitidis, V., and Purdy, K. J.: Nitrous
1049   oxide as a function of oxygen and archaeal gene abundance in the North Pacific, Nat Commun, 7, 13451,
1050   https://doi.org/10.1038/ncomms13451, 2016.

1051   Vaccaro, R. F. and Ryther, J. H.: Marine Phytoplankton and the Distribution of Nitrite in the Sea*, 25, 260–271,
1052   https://doi.org/10.1093/icesjms/25.3.260, 1960.

1053   Wada, E. and Hattori, A.: Nitrite metabolism in the euphotic layer of the central North Pacific Ocean, 16, 766–772,
1054   1971.

1055   Wada, E. and Hattori, A.: Nitrite distribution and nitrate reduction in deep sea waters, 19, 123–132,
1056   https://doi.org/10.1016/0011-7471(72)90044-7, 1972.

1057   Wan, X. S., Sheng, H.-X., Dai, M., Zhang, Y., Shi, D., Trull, T. W., Zhu, Y., Lomas, M. W., and Kao, S.-J.:
1058   Ambient nitrate switches the ammonium consumption pathway in the euphotic ocean, Nat Commun, 9, 915,
1059   https://doi.org/10.1038/s41467-018-03363-0, 2018.

1060   Wan, X. S., Sheng, H., Dai, M., Church, M. J., Zou, W., Li, X., Hutchins, D. A., Ward, B. B., and Kao, S.:
1061   Phytoplankton-nitrifier interactions control the geographic distribution of nitrite in the upper ocean, Global
1062   Biogeochem Cycles, https://doi.org/10.1029/2021GB007072, 2021.

1063   Ward, B. and Carlucci, A.: Marine ammonia-and nitrite-oxidizing bacteria: serological diversity determined by
1064   immunofluorescence in culture and in the environment, 50, 194–201, https://doi.org/10.1128/aem.50.2.194-
1065   201.1985, 1985.

1066   Ward, B. B.: Light and substrate concentration relationships with marine ammonium assimilation and oxidation
1067   rates, 16, 301–316, https://doi.org/10.1016/0304-4203(85)90052-0, 1985.

1068   Ward, B. B.: Temporal variability in nitrification rates and related biogeochemical factors in Monterey Bay,
1069   California, USA, Mar Ecol Prog Ser, 292, 97–109, https://doi.org/10.3354/meps292097, 2005.

1070   Ward, B. B., Olson, R. J., and Perry, M. J.: Microbial nitrification rates in the primary nitrite maximum off southern
1071   California, 29, 247–255, https://doi.org/10.1016/0198-0149(82)90112-1, 1982.

1072   Ward, B. B., Kilpatrick, K. A., Renger, E. H., and Eppley, R. W.: Biological nitrogen cycling in the nitracline, 34,
1073   493–513, https://doi.org/10.4319/lo.1989.34.3.0493, 1989.

1074   Watson, S. W. and Waterbury, J. B.: Characteristics of two marine nitrite oxidizing bacteria, Nitrospina gracilis nov.
1075   gen. nov. sp. and Nitrococcus mobilis nov. gen. nov. sp., 77, 203–230, 1971.

1076   Xu, M. N., Li, X., Shi, D., Zhang, Y., Dai, M., Huang, T., Glibert, P. M., and Kao, S.: Coupled effect of substrate
1077   and light on assimilation and oxidation of regenerated nitrogen in the euphotic ocean, Limnol Oceanogr, 64, 1270–
1078   1283, https://doi.org/10.1002/lno.11114, 2019.

1079   Yool, A., Martin, A. P., Fernández, C., and Clark, D. R.: The significance of nitrification for oceanic new
1080   production, 447, 999–1002, https://doi.org/10.1038/nature05885, 2007.

1081   Zafiriou, O. C., Ball, L. A., and Hanley, Q.: Trace nitrate in oxic waters, 39, 1329–1347,
1082   https://doi.org/10.1016/0198-0149(92)90072-2, 1992.

1083   Zakem, E. J., Al-Haj, A., Church, M. J., van Dijken, G. L., Dutkiewicz, S., Foster, S. Q., Fulweiler, R. W., Mills, M.
1084   M., and Follows, M. J.: Ecological control of nitrite in the upper ocean, 9, https://doi.org/10.1038/s41467-018-
1085   03553-w, 2018.

1086   Zehr, J. P. and Kudela, R. M.: Nitrogen Cycle of the Open Ocean: From Genes to Ecosystems, Annu. Rev. Mar.
1087   Sci., 3, 197–225, https://doi.org/10.1146/annurev-marine-120709-142819, 2011.

1088   Zehr, J. P. and Ward, B. B.: Nitrogen Cycling in the Ocean: New Perspectives on Processes and Paradigms, AEM,
1089   68, 1015–1024, https://doi.org/10.1128/AEM.68.3.1015-1024.2002, 2002.

1090

1096

Author Contributions

1098 Major data collection efforts, data processing/analysis and writing were conducted by N. Travis.
1099 Significant support during data collection was provided by C. Kelly and M. Mulholland, with additional
1100 contributions during manuscript editing. K. Casciotti was instrumental in initial project design, laboratory
1101 analysis, data investigations and manuscript writing.